Energy Reports 12 (2024) 381–401

Contents lists available at ScienceDirect

Energy Reports

journal homepage: www.elsevier.com/locate/egyr

Research paper

Observer based finite time sliding mode control strategies for single-stage grid-connected PV system with LCL filter

Ahmad Khan [a], Laiq Khan [a], Qudrat Khan [a], Zahid Ullah [b,*], Adil Latif [c]

[a] Department of Electrical and Computer Engineering, COMSATS University Islamabad, 45550, Islamabad, Pakistan
[b] Dipartimento di Elettronica, Informazione e Bioingegneria, Politecnico di Milano, 20133, Milano, Italy
[c] Department of Electrical and Computer Engineering, COMSATS University Islamabad, Abbottabad Campus, 22060, Abbottabad, Pakistan

ARTICLE INFO

Keywords:
Sliding mode
Photovoltaic
MPP
Grid connected
MATLAB
Simulink

ABSTRACT

The escalating global demand for clean and sustainable energy sources has trusted solar energy into the forefront of renewable energy (RE) solutions. Solar power generation, however, is profoundly influenced by ever-changing meteorological conditions, notably solar irradiation and temperature. These fluctuations have a direct impact on the voltage and current characteristics of photovoltaic arrays. To achieve optimal power transfer, a harmonious interface between the utility grid or load and solar panels is essential. In this research, the authors propose the integration of LCL filter to ameliorate harmonics emanating from inverter outputs. Additionally, a nonlinear control methodology is employed to maximize power extraction from Photovoltaic (PV) arrays at the Maximum Power Point (MPP) and to ensure a stable and less fluctuating injection of power into the grid. The primary goal of this work is to examine the effectiveness of nonlinear control techniques that assist in reducing harmonics and smoothing the output of solar power systems utilizing LCL filter. The controllers used here are nonlinear Super Twisting Reachability law-based Finite Time Sliding Mode Control (STR-FTSMC) and Arbitrary Order Finite Time Sliding Mode Control (AO-FTSMC) for the three-phase single-stage on-grid PV system in addition to sliding mode observer. The efficacy of the employed control techniques is highlighted via a comparative study in a MATLAB/Simulink environment.

1. Introduction

The widespread adoption of solar energy systems has fueled to anticipate the grid-connected photovoltaic (PV) systems that can harness the latest developments in control systems and power electronics technologies. In this context, voltage source inverters (VSIs) find common usage in a wide spectrum of power conversion applications, encompassing distributed generation (DG) systems rooted in PV technology, energy storage systems, wind turbines, and so on (Blaabjerg et al., 2006). The landscape of PV electricity generation is typically categorized into two primary domains: stand-alone and grid-connected systems. However, grid-connected systems, owing to their inherent advantages, emerged as the preferred choice for large-scale power generation endeavors. Notably, one significant advantage of grid-connected systems is their ability to operate without the necessity of high-capacity energy storage batteries (Menaga and Sankaranarayanan, 2020). This paper delves into the technical intricacies of these developments, presenting a comprehensive analysis of the advancements in control systems and power electronics, particularly within the context of grid-connected PV systems.

The preference for single-stage grid-connected PV systems over their two-stage counterparts can be attributed to several compelling factors. Notably, single-stage systems tend to offer a higher degree of cost-effectiveness by eliminating the need for an additional DC-DC converter stage, resulting in an overall reduction in system cost (Wu et al., 2011; Zeb et al., 2019). This cost-saving attribute is particularly advantageous for smaller-scale residential or commercial installations where budget constraints are crucial in decision-making. Furthermore, single-stage PV systems boast a simplified design and installation process. This streamlining of the installation procedure renders it more straightforward and less time-consuming. Although, two-stage systems may provide certain advantages in terms of optimizing power generation under varying solar conditions, a well-designed single-stage system can still deliver with sufficient efficiency for a wide array of applications. This paper provides an in-depth exploration of the merits of single-stage grid-connected PV systems, shedding light on their cost-effectiveness, simplicity of design, and suitability for various practical applications.

In the realm of grid-connected PV systems, two pivotal control objectives take central stage: maximizing PV power generation and

* Corresponding author.
E-mail address: zahid.ullah@polimi.it (Z. Ullah).

https://doi.org/10.1016/j.egyr.2024.05.069
Received 31 January 2024; Received in revised form 9 May 2024; Accepted 30 May 2024

minimizing harmonics in the inverter output voltage (Esram and Chapman, 2007). Achieving these goals is essential for ensuring the efficiency and reliability of PV systems. To attain maximum power point (MPP) operation, various control techniques have been devised. These include constant voltage control, the perturb and observe (P & O) algorithm, the incremental conductance algorithm, and their modified versions (Esram and Chapman, 2007). However, worth noting that implementing a multi-stage power conversion system, although it may offer certain advantages, introduces cost implications and can potentially compromise the dependability and overall energy efficiency of the PV installation (Rivera et al., 2017). For the reduction of harmonics, two types of filters are commonly employed: the L filter and the LCL filter. In this context, the LCL filter takes precedence due to its superior harmonic reduction capabilities compared to the L filter (Rivera et al., 2017). Augmenting these control strategies, nonlinear control techniques are leveraged to optimize power extraction from the PV system and seamlessly inject it into the grid (Wu et al., 2012; Beres et al., 2015; Bao et al., 2013). This paper provides a comprehensive exploration of the strategies and methodologies employed to achieve the dual objectives of maximizing PV power output and reducing harmonics in grid-connected PV systems.

In Mahmud et al. (2013), a three-phase single-stage grid-connected photovoltaic inverter system with non-linear control law is developed through an inclusive structure for the synchronous dq reference frame to track the maximum power regardless of climate conditions and to control active and reactive power without the use of extra power controller. Distributed generation and the incorporation of RES into the grid have both benefited from the advancement of power electronics technology. Nonlinear controllers deal directly with nonlinearities, there are various sophisticated and efficient nonlinear control approaches and schemes applied to grid-connected PV systems in the literature (Mahmud et al., 2013).

Sliding mode controllers (SMC) stand out as one of the most advanced control techniques, ensuring the fulfillment of control objectives even in the presence of nonlinearities, variations in model parameters, and external disturbances. Within the realm of grid-connected converters, SMC has garnered substantial attention due to its notable attributes, including rapid dynamic response, robustness, and excellent regulation qualities (Hao et al., 2012; Vieira et al., 2017; Komurcugil et al., 2015). This method finds significant applications in the control of grid-connected photovoltaic (PV) systems, as exemplified in Naddami and Ababssi (2023), Kim (2006, 2007). In the context of single-phase grid-connected systems (Kim, 2006), the focus is on achieving maximum power extraction, with a sliding mode controller devised based on current control. Similarly, in the case of three-phase grid-connected systems (Kim, 2007), integral sliding mode techniques are harnessed to craft the sliding surface, underscoring the versatility and effectiveness of SMC in achieving robust control objectives in grid-connected converter systems.

In Zeb et al. (2020, 2018), an investigation into the modeling and design of a Super Twisting Sliding Mode Controller (ST-SMC) is conducted, focusing on the efficient injection of both active and reactive power in a three-phase grid-connected PV system under various operating conditions, including abnormal scenarios. Furthermore, Huang et al. (2019) introduced an observer-based sliding mode control approach tailored for LCL-filtered grid-connected inverters, enhancing system stability. Notably, this control strategy minimizes the need for multiple state variable feedback, reducing sensor requirements by incorporating a state observer. The combination of a state observer with discrete sliding mode control in digital implementation streamlines the control architecture. Additionally, the utilization of estimated capacitor voltage within this framework contributes to active damping, effectively mitigating LCL resonance in the system. This research underscores the advancements in sliding mode control techniques, offering improved control and stability for grid-connected PV systems.

Yu et al. reviewed Terminal Sliding Mode Control (TSMC), including TSMC basics, TSMC developments, the state of art of TSMC theory, and its applications (Yu et al., 2020). The fundamental difference between the TSMC and conventional SMC has been investigated. The important features and advantages of TSMC have been analyzed, and the challenges in TSMC and their future trend in theory and applications have been outlined. Numerous control techniques have been devised for the efficient current control of LCL filter-based Grid-Connected Voltage Source Inverter (GC-VSI) systems. Among these, proportional-integral (PI) control (Jamil et al., 2020), repetitive control (RC) (Husev et al., 2019), proportional resonant (PR) control (Bo et al., 2009), and deadbeat control (DB) (Benyoucef et al., 2014) are the most common. Due to the inherent nonlinear nature of the LCL filter type GC-VSI system, these control techniques only achieved limited objectives and have their own merits and demerits. PI control is the simplest one; however, it suffers from poor sinusoidal current reference tracking performance and lack of disturbance rejection ability. Alternatively, various nonlinear controllers such as backstepping control, Lyapunov-based control, and SMC are being applied to meet the desired performance requirement. In Kale et al. (2016), continuous SMC is applied in the application of a shunt active filter to prevent distortive harmonics components due to high switching frequency.

Dehkordi et al. (2016) focused on a new harmonic and inter-harmonic compensation strategy proposed for DG-interfacing converters with LCL filters. The proposed method combines a backstepping control system based on a high order sliding mode differentiator. The controller aims to regulate the grid current, irrespective of the load dynamics, grid impedance, grid frequency, and grid voltage. To achieve the desirable performance and to reject any disturbance signal, a new backstepping control based on a high order sliding mode differentiator is proposed.

For improving the dynamic performance and quality of injected power of single stage single phase grid-connected photovoltaic system, a robust terminal mode control was designed (Chigane and Ouassaid, 2024). The model adapted for achieving improved dynamic performance helps the control of active as well as reactive power. For ensuing the voltage control of inverter under islanding condition, a robust SMC was designed (Barzegar-Kalashani et al., 2023). The proposed design was tested under different loading conditions as well as tested with different design parameters. This design showed fast transient response switching from no-load to full load and vice versa.

Voltage and current based Super twisting algorithm-sliding mode controller (STA-SMC) is interfaced with Distributed energy resources (DERs) designed for single-phase voltage sources inverter (Barzegar-Kalashani et al., 2022). The study was done for both grid connected and islanded operation incorporating the effect of load current and output voltage of filter as external disturbances. STA-SMC used, showed stability and robustness under different loading conditions. A novel SMC method for microgrid inverters, employing a compound reaching law to enhance voltage stability amidst load disturbances presented (Yuan et al., 2023). Adaptive SMC further mitigates disturbances, offering robust performance even with unknown disturbance boundaries. This approach significantly improves inverter system performance, making it promising for microgrid applications requiring precise voltage regulation under dynamic operating conditions.

1.1. Motivation and contributions

The main objective of this paper is to design and simulate the nonlinear control technique with a single-stage three-phase grid-connected photovoltaic system inverter and to extract the maximum power at MPP from PV by implementing the Maximum Power Point Tracking (MPPT) control technique. So, the system performance no longer remains appealing without a self-sufficient controller. For this purpose, Super Twisting Reachability law-based Finite Time Sliding Mode Control (STR-FTSMC) and Arbitrary Order Finite Time Sliding Mode Control

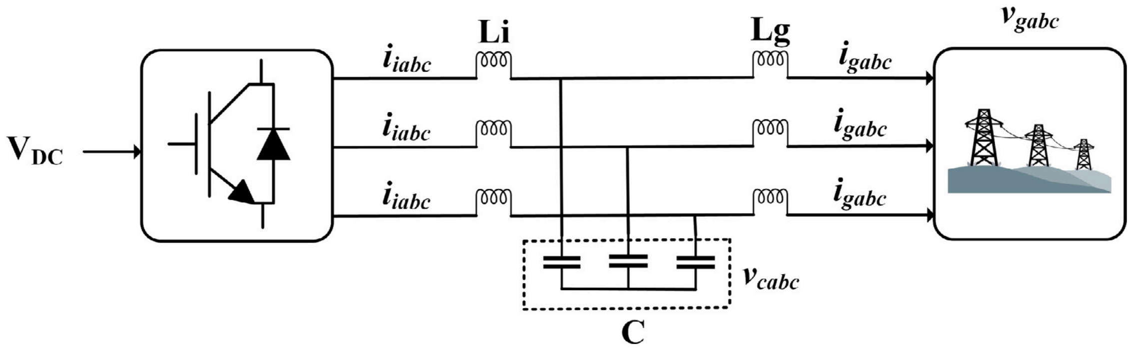

Fig. 1. Three-Phase inverter with LCL filter connected to Grid.

(AO-FTSMC) strategies will be adopted to perform robustly in uncertain scenarios. Sometimes system states are not available all the times so a state estimator will also be designed to provide the estimated states. As a result, the problem will be "observer-based finite-time sliding mode control strategies for grid-connected PV systems with LCL filter". The nonlinear control technique will extract the maximum power from the PV system and inject it into the grid.

1.2. Paper layout

The subsequent sections of the paper are structured as follows: Section 2 provides the mathematical modeling of three-phase grid connection and presents the problem formulation. In Section 3, we delve into the explanation of the proposed controller design. Section 4 is dedicated to present the results and engage in discussions regarding the proposed controller. Finally, the paper concludes with Section 5.

2. Mathematical modeling of three phase grid connected inverter with LCL filter

In this section, mathematical model for the proposed system is presented. Fig. 1 depicts a three phase grid connected model which consists of a PV system and an inverter that is connected to the grid through an LCL filter. An LCL filter is used to feed the grid with the inverter's output of AC power. By applying Kirchhoff's voltage and current law, the three-phase dynamic model of the system is obtained in stationary abc reference frame which is given as follows:

$$\left.\begin{aligned}
\frac{d}{dt}(v_{c_{abc}}) &= \frac{1}{C} i_{i_{abc}} - \frac{1}{C} i_{g_{abc}} \\
\frac{d}{dt}(i_{i_{abc}}) &= \frac{1}{L_i} v_{i_{abc}} - \frac{1}{L_i} v_{c_{abc}} \\
\frac{d}{dt}(i_{g_{abc}}) &= \frac{1}{L_g} v_{c_{abc}} - \frac{1}{L_g} v_{g_{abc}}
\end{aligned}\right\} \tag{1}$$

where $v_{c_{abc}}$ is the output voltage across the filter capacitor, C is output filter capacitance, $i_{i_{abc}}$ is the input current to the inverter, $i_{g_{abc}}$ is the grid current, $v_{i_{abc}}$ is the inverter input voltage, L_i, L_g are the output filter inductances and $v_{g_{abc}}$ is output grid voltage.

By using equations given in Appendix A, the system's dynamics (reported in Eq. (1)) are transformed into the following synchronously rotating dq-frame.

$$\Sigma : \begin{cases}
\dot{x}_1 = \frac{1}{L_g} x_2 + \omega x_4 - \frac{1}{L_g} v_{gd} \\
\dot{x}_2 = -\frac{1}{C} x_1 - \frac{1}{C} x_3 + \omega x_5 \\
\dot{x}_3 = -\frac{1}{L_i} x_2 + \omega x_6 + \frac{1}{L_i} d_d v_{dc} \\
\dot{x}_4 = \frac{1}{L_g} x_5 - \omega x_1 - \frac{1}{L_g} v_{gq} \\
\dot{x}_5 = -\frac{1}{C} x_4 + \frac{1}{C} x_6 - \omega x_2 \\
\dot{x}_6 = -\frac{1}{L_i} x_5 - \omega x_3 + \frac{1}{L_i} d_q v_{dc}
\end{cases} \tag{2}$$

where x_1, x_2 and x_3 are the d-component of grid current, capacitor voltage and inverter current, respectively. Similarly, x_4, x_5 and x_6 are the q-components of grid current, capacitor voltage and inverter current, respectively.

In addition, the control inputs are represented by $u_d = d_d v_{dc}$ and $u_q = d_q v_{dc}$. The dq model of Eq. (2) in compact form is given by:

$$\Sigma : \begin{cases}
\dot{x} = Ax + Bu \\
u = [u_d \ u_q]^T \\
y = h(x) = [i_{gd} \quad i_{gq}]
\end{cases} \tag{3}$$

where $x \in \mathbb{R}^m$, $u \in \mathbb{R}^l$ and $y \in \mathbb{R}^n$ are states, inputs and outputs vectors. A is the system distribution matrix and B is the input matrix. The fundamental goal of a three-phase grid-connected photovoltaic system is to supply the grid with a maximum amount of power from PV generation while maintaining a power factor of unity. The perturb and observe (P&O) MPPT algorithm gives $i_{ref} = i_{MPP} = i_{gdref}$ which is tracked by the proposed controller to inject maximum power into the grid. The i_{gqref} is set to zero to ensure power is injected at unity power factor.

3. Observer based sliding mode control techniques

In this section, the two control techniques i.e., STR-FTSMC and AO-FTSMC will be implemented.. The aim is to significantly increase power extraction from PV arrays under changing solar conditions while comparing with the existing control approaches. These approaches enable the PV system's operation in response to changing solar irradiation and temperature levels. They also maximize energy extraction by employing cutting-edge tracking algorithms and ensure precise navigation of the PV array to its MPP, in the presence of the environmental variations. Furthermore, the sliding mode control algorithms i.e., STR-FTSMC and AO-FTSMC are strong enough to withstand uncertainties and disruptions like rapid weather changes. Now, the observer and both the controllers will be presented in the proceeding subsection.

3.1. Sliding mode observer

The sliding-mode observer (also known as the Utkin observer) was introduced by Vadim I. Utkin in the late 1970s. This observer offers robustness to uncertainties, disturbances, and nonlinear dynamics by continuously driving the estimation error to the sliding surface. The key feature of utkin observer is the introduction of a switching function in the observer to achieve a sliding mode and steering of error dynamics to origin (Drakunov and Utkin, 1992). A general structure is shown as follows:

$$\dot{\hat{x}} = A\hat{x} + Bu + Ge_y + L\upsilon \tag{4}$$

where $e_y = [e_{y1}\ e_{y2}]^T$, such that $e_{y1} = (i_{gd} - \hat{i}_{gd})$ and $e_{y2} = (i_{gq} - \hat{i}_{gq})$. Where the core objective is to steer e_{y1} and e_{y2} to zero in finite time despite the nonlinearities (or uncertainties). Furthermore, G and L are in designer gains matrices and $\upsilon = k\,\text{sign}(e_y)$ such that $k \in \mathbb{R}^t$. The presence of υ ensures sliding mode in face of uncertainties i.e., enhance robustness to matched uncertainties.

The observer used is a full state observer which consists of G (proportional injecting term) and L (discontinuous term gain). By substituting matrices A, B, C, L, and G in Eq. (4), one gets the following expanded form.

$$\dot{\hat{x}}_1 = \frac{1}{L_g}\hat{x}_2 + \omega\hat{x}_4 + \left(L_{11}k_1\text{sign}(e_{y1}) + L_{12}k_2\text{sign}(e_{y2})\right) + (G_{11}e_{y1} + G_{12}e_{y2}) \tag{5}$$

$$\dot{\hat{x}}_2 = \frac{1}{C}\hat{x}_1 + \omega\hat{x}_5 + \frac{1}{C}\hat{x}_1 + \left(L_{21}k_1\text{sign}(e_{y1}) + L_{22}k_2\text{sign}(e_{y2})\right) + (G_{21}e_{y1} + G_{22}e_{y2}) \tag{6}$$

$$\dot{\hat{x}}_3 = \frac{1}{L_i}\hat{x}_2 + \omega\hat{x}_6 + \frac{1}{L_i}u_d + \left(L_{31}k_1\text{sign}(e_{y1}) + L_{32}k_2\text{sign}(e_{y2})\right) + (G_{31}e_{y1} + G_{32}e_{y2}) \tag{7}$$

$$\dot{\hat{x}}_4 = \frac{1}{L_g}\hat{x}_5 + \omega\hat{x}_1 + \left(L_{41}k_1\text{sign}(e_{y1}) + L_{42}k_2\text{sign}(e_{y2})\right) + (G_{41}e_{y1} + G_{42}e_{y2}) \tag{8}$$

$$\dot{\hat{x}}_5 = \frac{1}{C}\hat{x}_6 + \omega\hat{x}_2 + \frac{1}{C}\hat{x}_4 + \left(L_{51}k_1\text{sign}(e_{y1}) + L_{52}k_2\text{sign}(e_{y2})\right) + (G_{51}e_{y1} + G_{52}e_{y2}) \tag{9}$$

$$\dot{\hat{x}}_6 = \frac{1}{L_i}\hat{x}_5 + \omega\hat{x}_3 + \frac{1}{L_i}u_q + \left(L_{61}k_1\text{sign}(e_{y1}) + L_{62}k_2\text{sign}(e_{y2})\right) + (G_{61}e_{y1} + G_{62}e_{y2}) \tag{10}$$

where $\left[\dot{\hat{x}}_1\quad \dot{\hat{x}}_2\quad \dot{\hat{x}}_3\quad \dot{\hat{x}}_4\quad \dot{\hat{x}}_5\quad \dot{\hat{x}}_6\right]^T = \left[\dot{\hat{i}}_{gd}\quad \dot{\hat{\upsilon}}_{cd}\quad \dot{\hat{i}}_{id}\quad \dot{\hat{i}}_{gq}\quad \dot{\hat{\upsilon}}_{cq}\quad \dot{\hat{i}}_{iq}\right]^T$

This is expanded form of Utkin observer for the present system. The estimated states $\hat{x}_2$, $\hat{x}_3$, $\hat{x}_5$, $\hat{x}_6$ will be used in the control law.

Now, the employed control algorithms will be presented in the following paragraphs.

3.2. Super twisting reachability law based finite-time sliding mode control

Since, SMC is a well-known robust nonlinear control strategy that has a fast control action, better transient and steady-state performance and is invariant against matched uncertainties and disturbances when the system dynamics are in the sliding phase (Zhang et al., 2023). Finite-time sliding mode control is a control strategy that is used to design controllers for systems and render finite time convergence to the sliding surface.

3.2.1. Control design for d-component via SRF-TSMC

The d-component dynamics of the subsystem, Σ_1 are defined as:

$$\Sigma_1 : \begin{cases} \dot{x}_1 = \dfrac{1}{L_g}x_2 + \omega x_4 - \dfrac{1}{L_g}\upsilon_{gd} \\ \dot{x}_2 = -\dfrac{1}{C}x_1 - \dfrac{1}{C}x_3 + \omega x_5 \\ \dot{x}_3 = -\dfrac{1}{L_i}x_2 + \omega x_6 + \dfrac{1}{L_i}u_d \end{cases} \tag{11}$$

where $\left[x_1\quad x_2\quad x_3\right] = \left[i_{gd}\quad \upsilon_{cd}\quad i_{id}\right]$. The tracking error is defined as,

$$e_1 = x_1 - x_{1ref} \tag{12}$$

Taking time derivative of e_1, and incorporating Eq. (2), one has

$$\dot{e}_1 = \left(\frac{1}{L_g}x_2 + \omega x_4 - \frac{1}{L_g}\upsilon_{gd}\right) - \dot{x}_{1ref} \tag{13}$$

Now taking again time derivative of $\dot{e}_1$, and involving Eq. (2), one has

$$\ddot{e}_1 = \frac{1}{L_g}\left(-\frac{1}{C}x_1 + \frac{1}{C}x_3 + \omega x_5\right) + \omega\dot{x}_4 - \frac{1}{L_g}\dot{\upsilon}_{gd} - \ddot{x}_{1ref} \tag{14}$$

Taking the time derivative of Eq. (14), and using Eq. (2), one finally gets

$$\dddot{e}_1 = \frac{1}{L_g}\left(-\frac{1}{C}\left(\frac{1}{L_g}x_2 + \omega x_4 - \frac{1}{L_g}\upsilon_{gd}\right) + \frac{1}{C}\left(-\frac{1}{L_i}x_2 + \omega x_6 + \frac{1}{L_i}u_d\right) + \omega\dot{x}_5\right) + \omega\ddot{x}_4 - \frac{1}{L_g}\ddot{\upsilon}_{gd} - \dddot{x}_{1ref} \tag{15}$$

Remark 1. The generalized canonical form is a standard representation used in control system theory to describe the dynamics of nonlinear systems. It is particularly useful because it simplifies the analysis and design of control systems by expressing them in a control convenient form. In the context of our study, the canonical form allows us to represent the dynamics of the control system in a structured manner, making it easier to analyze and design control strategies such as the STR-FTSMC and AO-FTSMC. Specifically, the canonical form helps in understanding the relationships between the system's inputs, outputs, and states, facilitating the development of effective control algorithms.

To develop canonical form, the following transformation may be defined. So, eventually, one gets the following

$$\left.\begin{aligned} \dot{e}_{11} &= e_{12} \\ \dot{e}_{12} &= e_{13} \\ \dot{e}_{13} &= f_1(x_1, x_2, x_3) + g_1 u \end{aligned}\right\} \tag{16}$$

where

$$f_1(x_1, x_2, x_3) = \frac{1}{L_g}\left(-\frac{1}{C}\left(\frac{1}{L_g}x_2 + \omega x_4 - \frac{1}{L_g}\upsilon_{gd}\right) + \frac{1}{C}\left(-\frac{1}{L_i}x_2 + \omega x_6\right) + \omega\dot{x}_5\right) + \omega\ddot{x}_4 - \frac{1}{L_g}\ddot{\upsilon}_{gd} - \dddot{x}_{1ref} \text{ and } g_1 = \frac{1}{L_i C L_g}$$

Now, the control convenient form is ready. Therefore, the sliding surface, s_1 is defined as:

$$s_1 = e_{12} + C_1 e_{11} \tag{17}$$

where C_1 is a positive constant. Now, the first and second time derivative of Eq. (17) along Eq. (16) are given by

$$\dot{s}_1 = e_{13} + C_1 e_{12} \tag{18}$$

and

$$\ddot{s}_1 = \dot{e}_{13} + C_1 e_{13} \tag{19}$$

Now based on surface s_1, a final sliding surface is defined as

$$s_d = \dot{s}_1 + \alpha_1 s_1 \tag{20}$$

The time derivative of Eq. (20) (i.e., $\dot{s}_d = \ddot{s}_1 + \alpha_1 \dot{s}_1$), along Eqs. (17)–(19), is given by

$$\dot{s}_d = \dot{e}_{13} + e_{13}(C_1 + \alpha_1) + \alpha_1 C_1 e_{12} \tag{21}$$

Comparing Eqs. (21) along Eqs. (16), one has

$$\dot{s}_d = \frac{1}{L_g}\left(-\frac{1}{C}\left(\frac{1}{L_g}x_2 + \omega x_4 - \frac{1}{L_g}v_{gd}\right) + \frac{1}{C}\left(-\frac{1}{L_i}x_2 + \omega x_6\right) + \omega \dot{x}_5\right) + \omega \ddot{x}_4 - \frac{1}{L_g}\ddot{v}_{gd} - \ddot{x}_{1ref} + \frac{u_d}{L_i C L_g} + e_{13}(C_1 + \alpha_1) + \alpha_1 C_1 e_{12} \tag{22}$$

Using the general structure of super twisting control law (Levant, 1993)

$$\dot{s}_d = -A_1 \mathrm{sign}(s_d) - A_1 \int_0^t \mathrm{sign}(s_d)dt \tag{23}$$

By equating Eqs. (22) and (23) and solving for u_d, one gets Eq. (24)

Remark 2. This system under study is linear in input, output, and states. So, it supports the separation principles. Therefore, the stabilities of the observer and control components are proved in the respective section. In the implementation context, the states in the d and q-components are replaced by the estimated states which support the theory.

$$u_d = L_i C L_g\left(-\frac{1}{L_g}\left(-\frac{1}{C}\left(\frac{1}{L_g}\hat{x}_2 + \omega x_4 - \frac{1}{L_g}v_{gd}\right) + \frac{1}{C}\left(-\frac{1}{L_i}\hat{x}_2 + \omega \hat{x}_6\right) + \omega \dot{x}_5\right)\right) - \omega \ddot{x}_4 + \frac{1}{L_g}\ddot{v}_{gd} + \ddot{x}_{1ref} - e_{13}(C_1 + \alpha_1) - \alpha_1 C_1 e_{12} - A_1 \mathrm{sign}(s_d) - A_1 \int_0^t \mathrm{sign}(s_d)dt \tag{24}$$

This is the required control law for the d-component. The design for the q-component will be outlined in the following study.

3.2.2. Control design for q-component via finite time sliding mode controller

The q-component dynamics of the subsystem, Σ_2 are defined as:

$$\Sigma_2 : \begin{cases} \dot{x}_4 = \frac{1}{L_g}x_5 - \omega x_1 - \frac{1}{L_g}v_{gq} \\ \dot{x}_5 = -\frac{1}{C}x_4 + \frac{1}{C}x_6 - \omega x_2 \\ \dot{x}_6 = -\frac{1}{L_i}x_5 - \omega x_3 + \frac{1}{L_i}u_q \end{cases} \tag{25}$$

where $\begin{bmatrix} x_4 & x_5 & x_6 \end{bmatrix} = \begin{bmatrix} i_{gq} & v_{cq} & i_{iq} \end{bmatrix}$. The tracking error is defined as,

$$e_2 = x_4 - x_{4ref} \tag{26}$$

Taking time derivative of e_2, and incorporating Eq. (2), one has

$$\dot{e}_2 = \left(\frac{1}{L_g}x_5 - \omega x_1 - \frac{1}{L_g}v_{gq}\right) - \dot{x}_{4ref} \tag{27}$$

Now taking again time derivative of $\dot{e}_2$, and involving Eq. (2), one has

$$\ddot{e}_2 = \frac{1}{L_g}\left(-\frac{1}{C}x_4 + \frac{1}{C}x_6 - \omega x_2\right) - \omega \dot{x}_1 - \frac{1}{L_g}\dot{v}_{gq} - \ddot{x}_{4ref} \tag{28}$$

Taking the time derivative of Eq. (28), and using Eq. (2), one finally gets

$$\dddot{e}_2 = \frac{1}{L_g}\left(-\frac{1}{C}\left(\frac{1}{L_g}x_5 - \omega x_1 - \frac{1}{L_g}v_{gq}\right) + \frac{1}{C}\left(-\frac{1}{L_i}x_5 - \omega x_3 + \frac{1}{L_i}u_q\right) - \omega \dot{x}_2\right) - \omega \ddot{x}_1 - \frac{1}{L_g}\ddot{v}_{gq} - \dddot{x}_{4ref} \tag{29}$$

To develop canonical form, the following transformation may be defined. So, eventually, one gets the following

$$\left.\begin{aligned} \dot{e}_{21} &= e_{22} \\ \dot{e}_{22} &= e_{23} \\ \dot{e}_{23} &= f_2(x_4, x_5, x_6) + g_2 u \end{aligned}\right\} \tag{30}$$

where

$$f_2(x_4, x_5, x_6) = \frac{1}{L_g}\left(-\frac{1}{C}\left(\frac{1}{L_g}x_5 - \omega x_1 - \frac{1}{L_g}v_{gq}\right) + \frac{1}{C}\left(-\frac{1}{L_i}x_5 - \omega x_3\right) - \omega \dot{x}_2\right) - \omega \ddot{x}_1 - \frac{1}{L_g}\ddot{v}_{gq} - \dddot{x}_{4ref} \text{ and } g_2 = \frac{1}{L_i C L_g}$$

Now, the control convenient form is ready. Therefore, the sliding surface, s_2 is defined as:

$$s_2 = e_{22} + C_2 e_{21} \tag{31}$$

where C_2 is a positive constant. Now, the first and 2nd time derivative of Eq. (31) along Eq. (30) are given by

$$\dot{s}_2 = e_{23} + C_2 e_{22} \tag{32}$$

and

$$\ddot{s}_2 = \dot{e}_{23} + C_2 e_{23} \tag{33}$$

Now based on surface s_2, a final sliding surface is defined as

$$s_q = \dot{s}_2 + \alpha_2 s_2 \tag{34}$$

The time derivative of Eq. (34) (i.e., $\dot{s}_q = \ddot{s}_2 + \alpha_2 \dot{s}_2$), along Eqs. (31)–(33), is given by

$$\dot{s}_q = \dot{e}_{23} + e_{23}(C_2 + \alpha_2) + \alpha_2 C_2 e_{22} \tag{35}$$

Comparing Eqs. (35) along Eqs. (30), one has

$$\dot{s}_q = \frac{1}{L_g}\left(-\frac{1}{C}\left(\frac{1}{L_g}x_5 + \omega x_1 - \frac{1}{L_g}v_{gq}\right) + \frac{1}{C}\left(-\frac{1}{L_i}x_5 + \omega x_3\right) + \omega x_5\right) + \omega \ddot{x}_1 - \frac{1}{L_g}\ddot{v}_{gq} - \dddot{x}_{4ref} + \frac{u_q}{L_i C L_g} + e_{23}(C_2 + \alpha_2) + \alpha_2 C_2 e_{22} \tag{36}$$

Using the general structure of super twisting control law as:

$$\dot{s}_q = -A_2 \mathrm{sign}(s_q) - A_2 \int_0^t \mathrm{sign}(s_q)dt \tag{37}$$

By equating Eqs. (36) and (37) and solving for u_d, one gets Eq. (38) according to Remark 2.

$$u_q = L_i C L_g\left(-\frac{1}{L_g}\left(-\frac{1}{C}\left(\frac{1}{L_g}\hat{x}_5 + \omega x_1 - \frac{1}{L_g}v_{gq}\right) + \frac{1}{C}\left(-\frac{1}{L_i}\hat{x}_5 + \omega \hat{x}_3\right) + \omega \dot{x}_2\right)\right) - \omega \ddot{x}_1 + \frac{1}{L_g}\ddot{v}_{gq} + \dddot{x}_{4ref} - e_{23}(C_2 + \alpha_2) - \alpha_2 C_2 e_{22} - A_2 \mathrm{sign}(s_q) - A_2 \int_0^t \mathrm{sign}(s_q)dt \tag{38}$$

This is the required control law for the q-component. Now in the next section, another control design method is discussed.

3.3. Arbitrary order finite time sliding mode controller

The Arbitrary Order Finite Time Sliding Mode Controller (AO-FTSMC) is a control strategy that aims to achieve robustness and fast convergence of the control system in a finite time. The advantage of Arbitrary Order sliding mode control (SMC) is its adaptability to diverse system dynamics and performance needs. Unlike fixed-order SMC, it offers greater flexibility in handling complex systems with uncertain or time-varying dynamics. The key advantage of AO-FTSMC is the establishment of finite time sliding mode as well as the finite time convergence of the error dynamics to zero. This, in turn, results in high precision which is ever demanded in control designs. Now, for the sake of completion, the design for d-components of the system will be presented and the q-components design can be carried out in similar fashion as that of d-component.

3.3.1. Design of d-component and q-component of AO-FTSMC

The AO-FTSMC is also a sliding mode based strategy (Alam et al., 2020). However, it is design differs from conventional SMC in the sliding surface. The sliding surface is designed in such a way that it facilitates finite time sliding mode enforcement as well as, after sliding mode establishment, it results in the finite time convergence error dynamics. As mentioned earlier the finite time convergence results in high precision while retaining the Key features of SMC.

At this stage, the sliding surface for the d-component for the controller is defined as:

$$s_d = e_{13} + e_{12} + e_{11} + \int_0^t (b_{13}|e_{13}|^{\alpha_{13}}\mathrm{sign}(e_{13})) + (b_{12}|e_{12}|^{\alpha_{12}}\mathrm{sign}(e_{12})) + (b_{11}|e_{11}|^{\alpha_{11}}\mathrm{sign}(e_{11})) + (c_{13}|e_{13}|^{\beta_{13}}\mathrm{sign}(e_{13})) + (c_{12}|e_{12}|^{\beta_{12}}\mathrm{sign}(e_{12})) + (c_{11}|e_{11}|^{\beta_{11}}\mathrm{sign}(e_{11}))dt \tag{39}$$

The reachability condition for the d-component for the control law is used as follows

$$\dot{s}_d = k_{11}\mathrm{sign}(s_d) + k_{12}|s_d|^{\alpha_1}\mathrm{sign}(s_d) + k_{13}|s_d|^{\gamma_1}\mathrm{sign}(s_d) + k_{14}(s_d) \tag{40}$$

The time derivative of Eq. (39) becomes

$$\dot{s}_d = \dot{e}_{13} + \dot{e}_{12} + \dot{e}_{11} + (b_{13}|e_{13}|^{\alpha_{13}}\mathrm{sign}(e_{13})) + (b_{12}|e_{12}|^{\alpha_{12}}\mathrm{sign}(e_{12})) + (b_{11}|e_{11}|^{\alpha_{11}}\mathrm{sign}(e_{11})) + (c_{13}|e_{13}|^{\beta_{13}}\mathrm{sign}(e_{13})) + (c_{12}|e_{12}|^{\beta_{12}}\mathrm{sign}(e_{12})) + (c_{11}|e_{11}|^{\beta_{11}}\mathrm{sign}(e_{11})) \tag{41}$$

Now, making use of Eq. (16) in Eq. (41), then comparing and solving for u_d, one gets

$$u_d = L_i C L_g \left(-\frac{1}{L_g}\left(-\frac{1}{C}\left(\frac{1}{L_g}\hat{x}_2 + \omega x_4 - \frac{1}{L_g}v_{gd}\right) + \frac{1}{C}\left(-\frac{1}{L_i}\hat{x}_2 + \omega\hat{x}_6\right) + \omega\dot{x}_5\right)\right) - \omega\ddot{x}_4 + \frac{1}{L_g}\ddot{v}_{gd} + \ddot{x}_{1ref} - \dot{e}_{12} - \dot{e}_{11} - (b_{13}|e_{13}|^{\alpha_{13}}\mathrm{sign}(e_{13})) - (b_{12}|e_{12}|^{\alpha_{12}}\mathrm{sign}(e_{12})) - (b_{11}|e_{11}|^{\alpha_{11}}\mathrm{sign}(e_{11})) - (c_{13}|e_{13}|^{\beta_{13}}\mathrm{sign}(e_{13})) - (c_{12}|e_{12}|^{\beta_{12}}\mathrm{sign}(e_{12})) - (c_{11}|e_{11}|^{\beta_{11}}\mathrm{sign}(e_{11})) + k_{11}\mathrm{sign}(s_d) + k_{12}|s_d|^{\alpha_1}\mathrm{sign}(s_d) + k_{13}|s_d|^{\gamma_1}\mathrm{sign}(s_d) + k_{14}(s_d) \tag{42}$$

Eq. (42) gives the final structure of the controller for d-component. While for the q-component, the control law is given by Eq. (43)

$$u_q = L_i C L_g \left(-\frac{1}{L_g}\left(-\frac{1}{C}\left(\frac{1}{L_g}\hat{x}_5 + \omega x_1 - \frac{1}{L_g}v_{gq}\right) + \frac{1}{C}\left(-\frac{1}{L_i}\hat{x}_5 + \omega\hat{x}_6\right) + \omega\dot{x}_2\right)\right) - \omega\ddot{x}_1 + \frac{1}{L_g}\ddot{v}_{gq} + \ddot{x}_{4ref} - \dot{e}_{22} - \dot{e}_{21} - (b_{23}|e_{23}|^{\alpha_{23}}\mathrm{sign}(e_{23})) - (b_{22}|e_{22}|^{\alpha_{22}}\mathrm{sign}(e_{22})) - (b_{21}|e_{21}|^{\alpha_{21}}\mathrm{sign}(e_{21})) - (c_{23}|e_{23}|^{\beta_{23}}\mathrm{sign}(e_{23})) - (c_{22}|e_{22}|^{\beta_{22}}\mathrm{sign}(e_{22})) - (c_{21}|e_{21}|^{\beta_{21}}\mathrm{sign}(e_{21})) + k_{21}\mathrm{sign}(s_q) + k_{22}|s_q|^{\alpha_2}\mathrm{sign}(s_q) + k_{23}|s_q|^{\gamma_2}\mathrm{sign}(s_q) + k_{24}(s_q) \tag{43}$$

Now, both the control algorithms are presented elaborately. The closed loop stability presentation is omitted here. However, the readers are referred to study (Ullah et al., 2020).

4. Simulation and results

The performance of the proposed controllers is evaluated using numerical simulation with MATLAB/Simulink. The block diagram of the simulation is depicted in Fig. 2. The system consists of a PV array and an inverter that is connected to the grid through LCL filter. A controller is fed by i_{ref} which is given by MPPT algorithm for maximum power tracking and the grid outputs after conversion from abc to direct quadrature zero ($dq0$) frame. The controller output is then converted back to abc and supplied to the inverter through a PWM module. Phase locked loop (PLL) has been utilized so as to synchronize the voltage of inverter with grid voltage. The internal diagram of PLL is depicted in Fig. 3 and the internal block diagram for STR-FTSMC and AO-FTSMC is shown in Figs. 5–8.

In this section, the proposed control system design is analyzed using output current, voltage, active power, reactive power, and total harmonic distortion are monitored for the two controllers to conduct comparative analysis. A comparison of the proposed control strategies with existing MPPT algorithms such as P&O based PI shown in Fig. 4 will be performed to assess their efficiency and reliability in maximizing power extraction at the MPP. It is observed that the proposed STR-FTSMC and AO-FTSMC control strategies outperform existing P&O based PI MPPT algorithm for varying atmospheric conditions. The simulation results of STR-FTSMC and AO-FTSMC are comprehensively discussed. The system parameters are listed in Table 1.

The incorporation of the super twisting reach-ability rule into the STR-FTSMC method considerably improves the robustness of grid-connected PV system, especially in circumstances of abrupt weather changes. The control technique guarantees speedy and precise tracking of the required trajectories, even under dynamic operating conditions, by utilizing the inherent robustness of the super twisting algorithm to uncertainties and disturbances. Specifically, during abrupt weather changes, the super twisting reach-ability rule allows for rapid adjustments in control inputs to preserve stable operation and reduce the impact of disruptions on system performance. The exploration of arbitrary order finite time sliding mode control (AO-FTSMC) prompts investigation into how the sliding surface order affects convergence speed. Higher orders may yield faster convergence but heightened sensitivity to uncertainties, while lower orders offer improved robustness but slower convergence. We acknowledge that the use of advanced control approaches may complicate system design and necessitate careful parameter tweaking. The LCL filter parameters are given in Table 2.

The variable irradiance has been applied to the solar panels to get varying PV output. Solar irradiance changes with time as shown in Fig. 9. Irradiance varies for 24 h, maximum in day light and minimum during night time. Variation in irradiance causes a change in current and power. Irradiance has a positive effect on current as well as power i.e., power changes as the current varies according to change in irradiance. The results of two different controllers are given in the next sub sections i.e., Section 4.1 for the results of STR-FTSMC and Section 4.3 for the results of AO-FTSMC.

4.1. Simulation results of STR-FTSMC

The parameters of the given controller are listed in Table 3.

As irradiance changes, the grid current also changes following the behavior of the irradiance profile. Fig. 10 illustrates the output of the PV power as the controller tracks the irradiance change over time which results in tracking the reference power.

The grid voltage and current are in phase as shown in Fig. 11, which demonstrates that the power factor of the grid power is unity. When

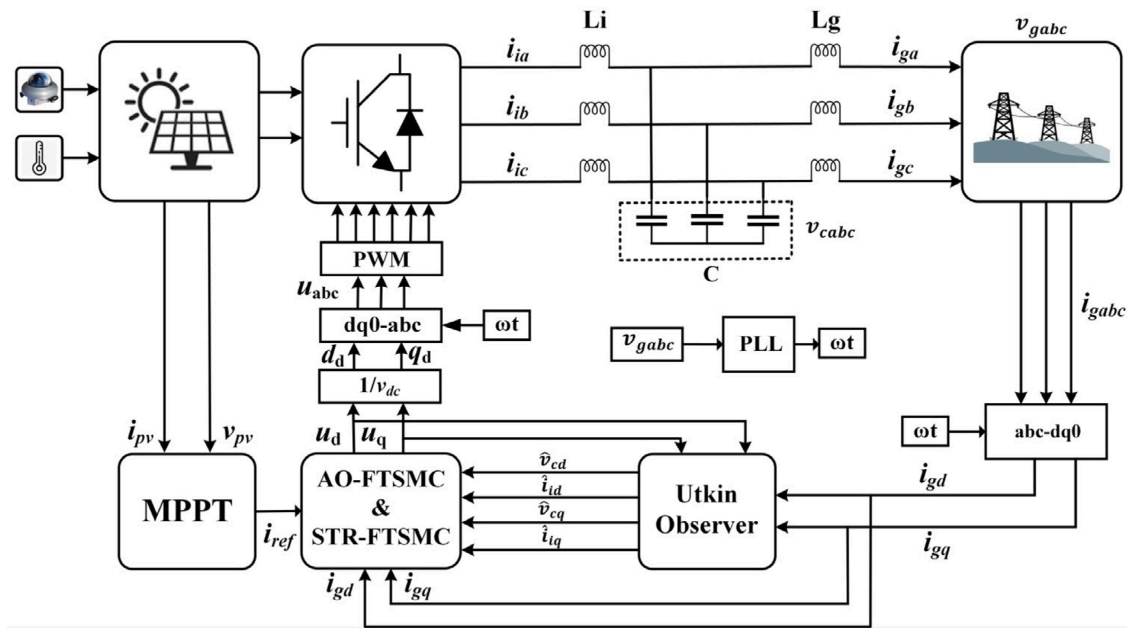

Fig. 2. Block diagram of the overall system.

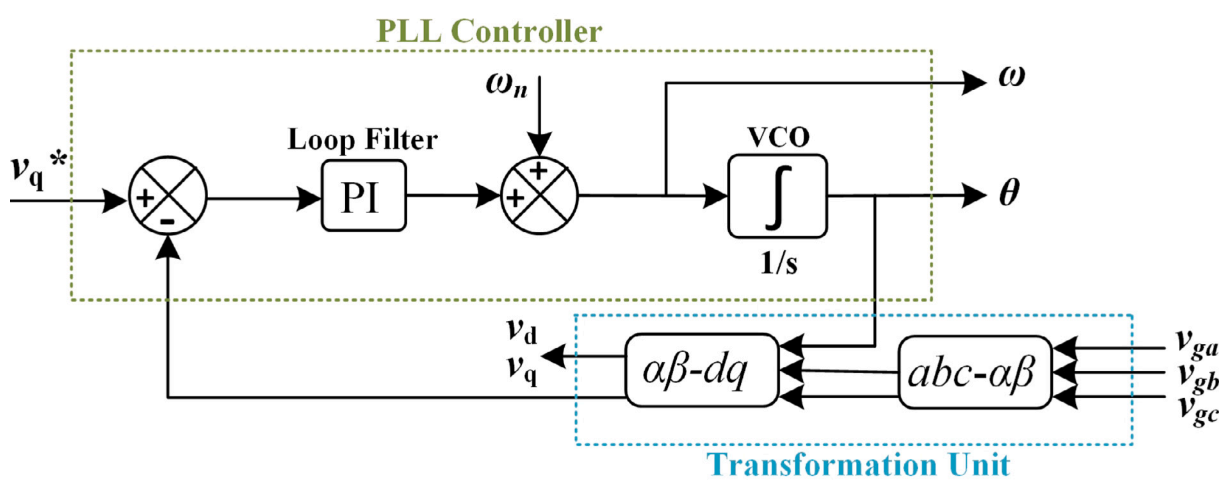

Fig. 3. Internal diagram of PLL.

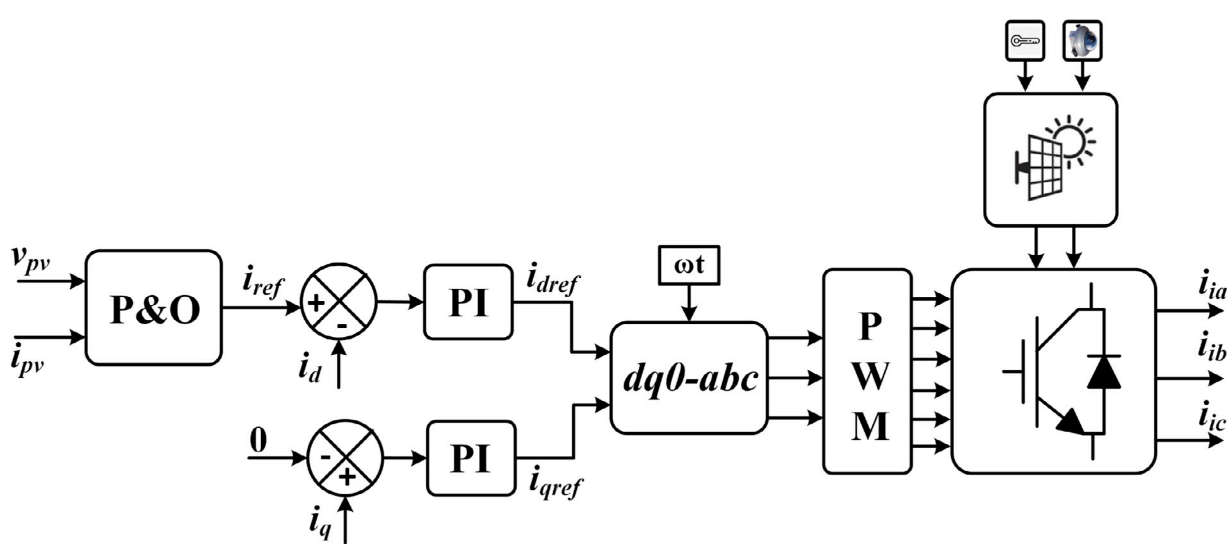

Fig. 4. P&O based PI.

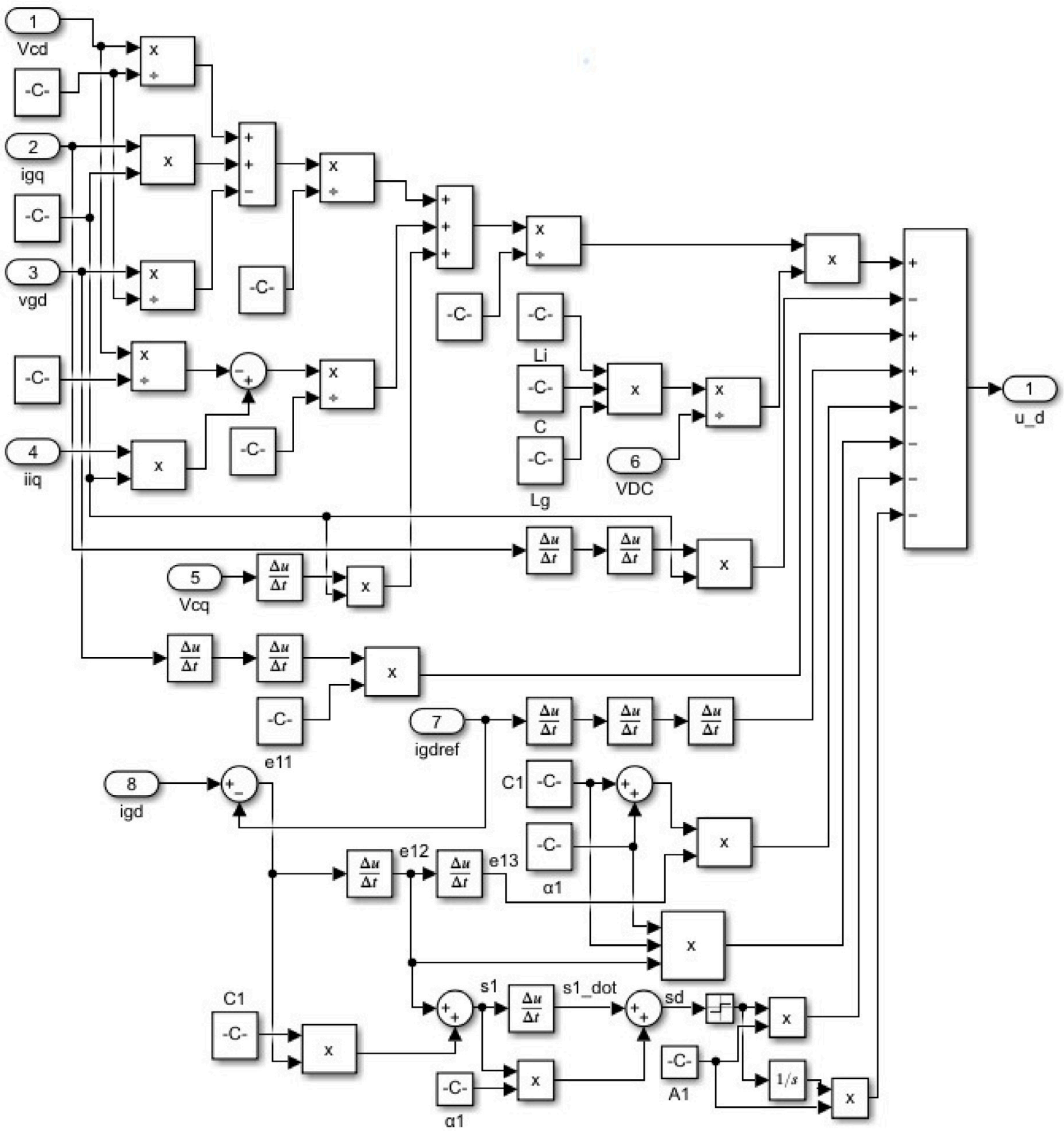

Fig. 5. Internal block diagram for u_d STR-FTSMC.

Table 1
System parameters.

Name of parameters	Values	Units
Parallel strings	11	
Series-connected module per string	21	
Module	SunPower SPR-230NE-BLK-U-ACPV	
Maximum power	230.04	W
Cells per module	72	
Open circuit voltage	48.2	V
Short-circuit current	6.05	A
Voltage at maximum power point	40.5	V
Current at maximum power point	5.68	A
Temperature coefficient of V_{oc}	−0.252	(%/deg. C)
Temperature coefficient of I_{sc}	0.039008	(%/deg. C)

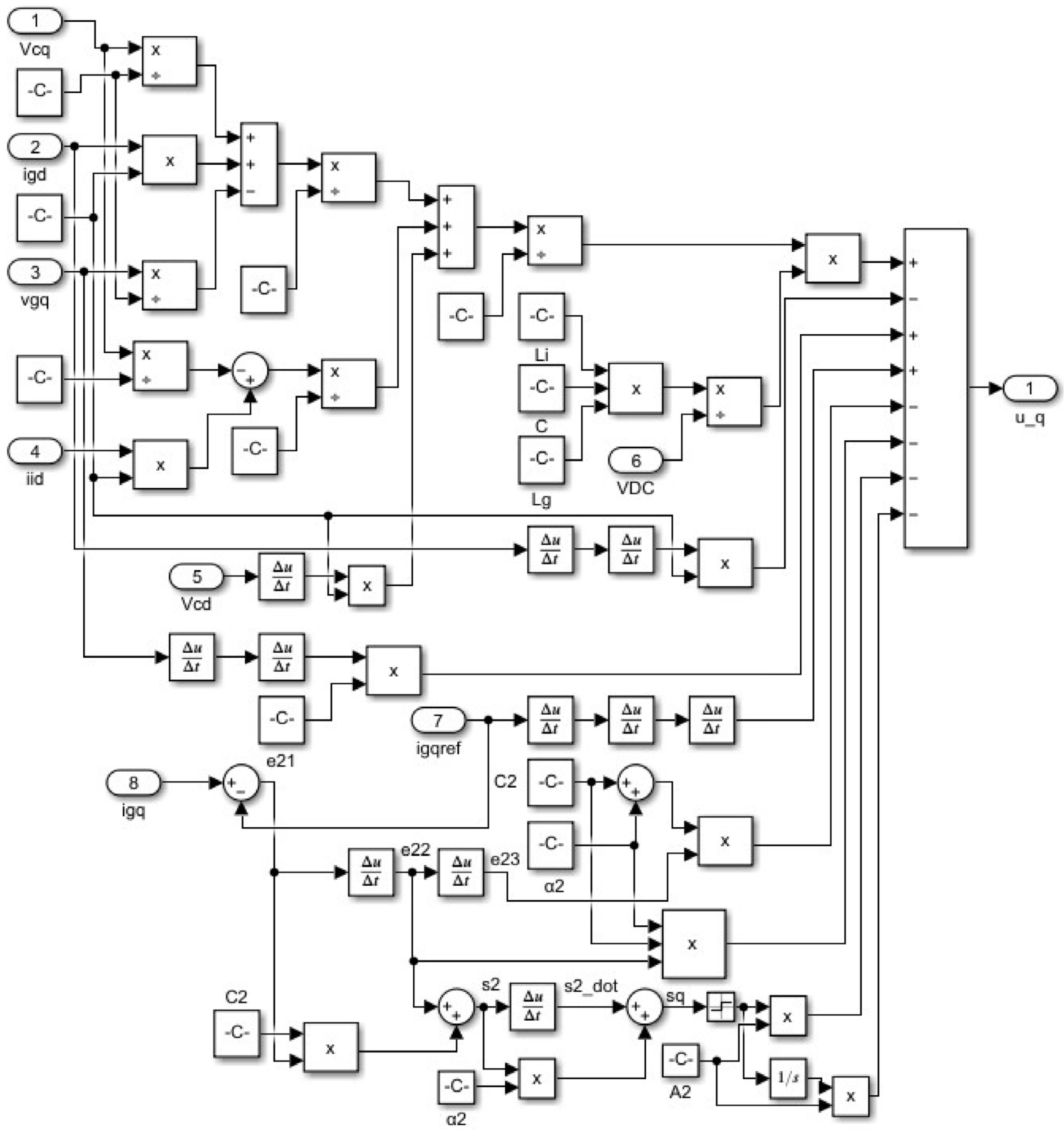

Fig. 6. Internal block diagram for u_q STR-FTSMC.

Table 2
LCL filter parameters.

Parameters	Value
Inductance (L_i)	7 mH
Capacitance (C)	0.1 μF
Inductance (L_g)	7 mH

Table 3
Parameters of STR-FTSMC.

u_d	Value	u_q	Value
A_1	100	A_2	100
α_1	0.9	α_2	0.9
C_1	0.8	C_2	0.8

current and voltage are in phase, their maximum and minimum values occur simultaneously. Fig. 12 displays active power, indicating that the grid has received the maximum amount of real power. The reactive component of power, however, becomes zero as the i_q reference is set to zero.

With STR-FTSMC, fewer harmonics are generated and shows variation when the irradiance changes and the THD with STR-FTSMC has been shown in Fig. 13.

4.2. Observer-based STR-FTSMC

i_{gd}, the d-component of the grid current, and i_{gq}, the q-component of the grid current, are the two states that will be used as the observer's inputs. Under the suggested controller, v_{cd}, v_{cq}, $\hat{i}_{id}$ and $\hat{i}_{iq}$ have been estimated. The observer's states are compared to the system's actual states while using the suggested control method.

An observer using the proposed technique, STR-FTSMC, accurately estimates all the states. The observed as well as actual states are shown

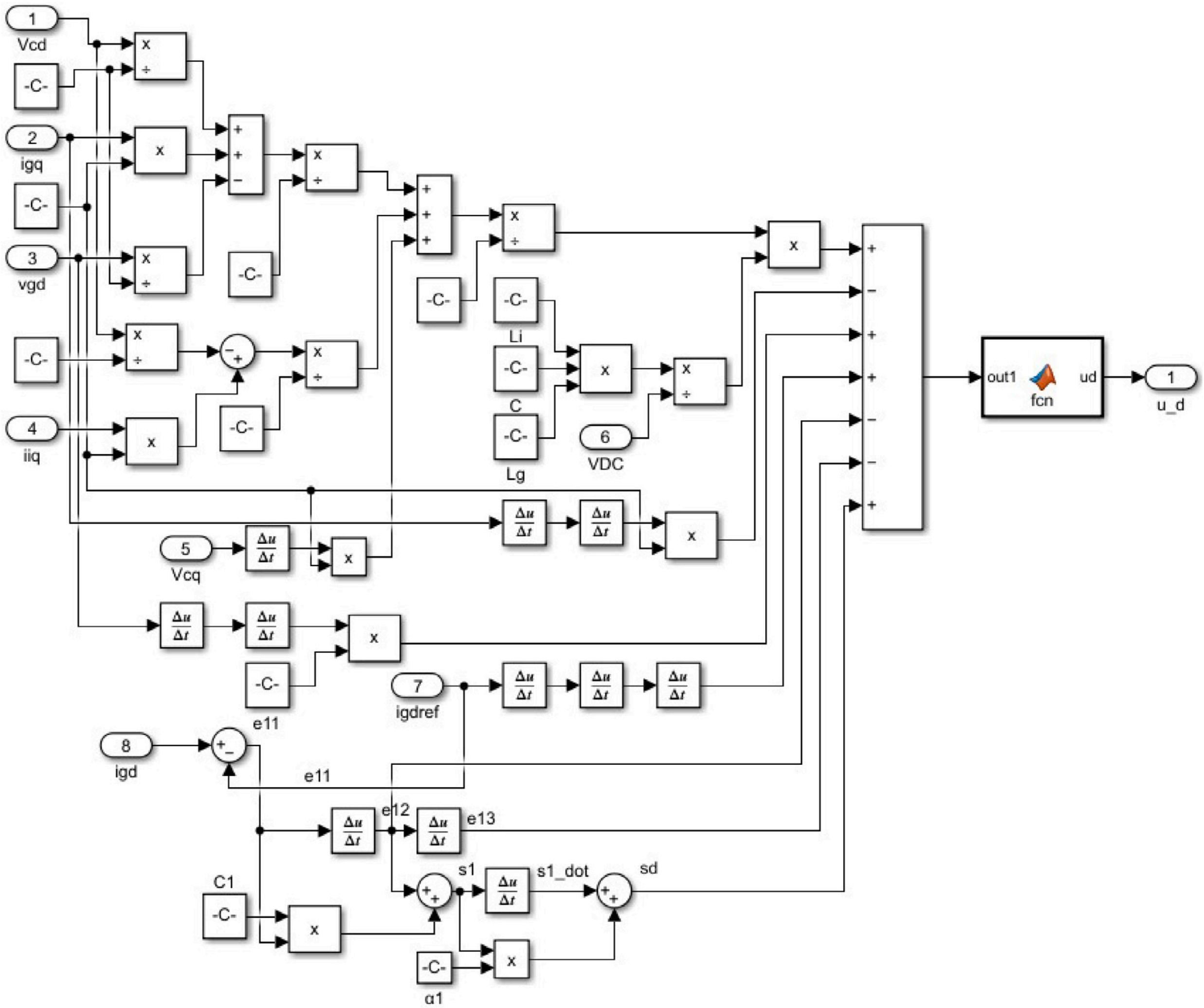

Fig. 7. Internal block diagram for u_d AO-FTSMC.

Table 4
Parameters of AO-FTSMC.

u_d	Value	u_d	Value	u_q	Value	u_q	Value
k_{11}	100	β_{13}	1.5	k_{21}	10	β_{23}	1.7
k_{12}	50	b_{11}	40	k_{22}	500	b_{21}	10
k_{13}	100	b_{12}	10	k_{23}	300	b_{22}	10
k_{14}	100	b_{13}	30	k_{24}	100	b_{23}	10
α_{11}	0.9	c_{11}	20	α_{21}	0.7	c_{21}	20
α_{12}	0.1	c_{12}	10	α_{22}	0.3	c_{22}	10
α_{13}	0.1	c_{13}	20	α_{23}	0.3	c_{23}	20
β_{11}	1.5	α_1	0.7	β_{21}	1.5	α_2	0.2
β_{12}	1.5	γ_1	0.3	β_{22}	1.7	γ_2	0.4

in Figs. 14–19. The states $\hat{x}_2$, $\hat{x}_3$, $\hat{x}_4$, $\hat{x}_5$ and $\hat{x}_6$ are used in the control law.

4.3. Simulation results of AO-FTSMC

The simulation results of AO-FTSMC are illustrated for a three-phase grid-connected PV system in this section. Table 4 shows the parameters for the controller which can be used for tunning the controller.

An arbitrary order finite-time SMC is designed for a three-phase grid-connected PV system by adding some special non-linear terms in the control law. These terms ensure that the sliding mode is enforced in a fixed time, which do not depend on the initial conditions. This improves the robustness and performance of the controller.

Fig. 20 illustrates the output of the PV power as the controller follows the irradiance change over time which resulting in AO-FTSMC accurately tracks the reference power.

Fig. 21 shows a phase of grid voltage and current, which are in phase. The in-phase grid voltage and grid current prove that power factor of grid is unity. Current and voltage are in phase means that they reach their maximum and minimum values at the same time. This is desirable when injecting current into the grid, because, it ensures that the active power delivered by the source is equal to the power injected into the grid.

Fig. 22 shows active and reactive power as the maximum real power has been delivered to the grid. The figure also shows an increase in active power when the irradiance increases and vice versa. However, the reactive power is zero as i_q reference is set to zero, and the reactive component of power becomes zero.

The controller AO-FTSMC shows better harmonic distortion which is less than 5% according to the IEEE standard 519. Fig. 23 shows fewer harmonics and shows variation when the irradiance changes.

4.4. Observer-based AO-FTSMC

The two states which will be used as input to the observer are i_{gd} (d-component of grid current) and i_{gq} (q-component of grid current).

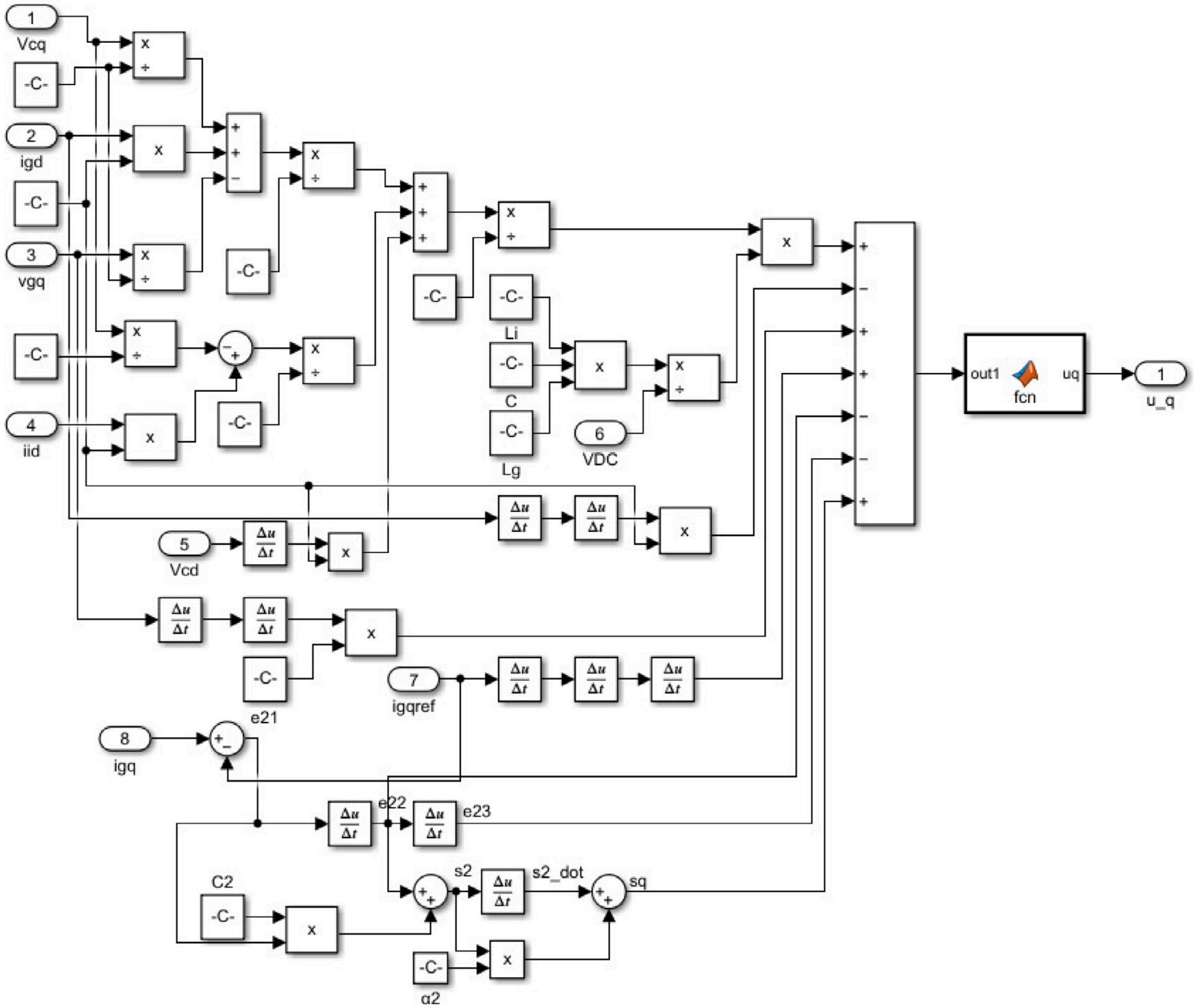

Fig. 8. Internal block diagram for u_q AO-FTSMC.

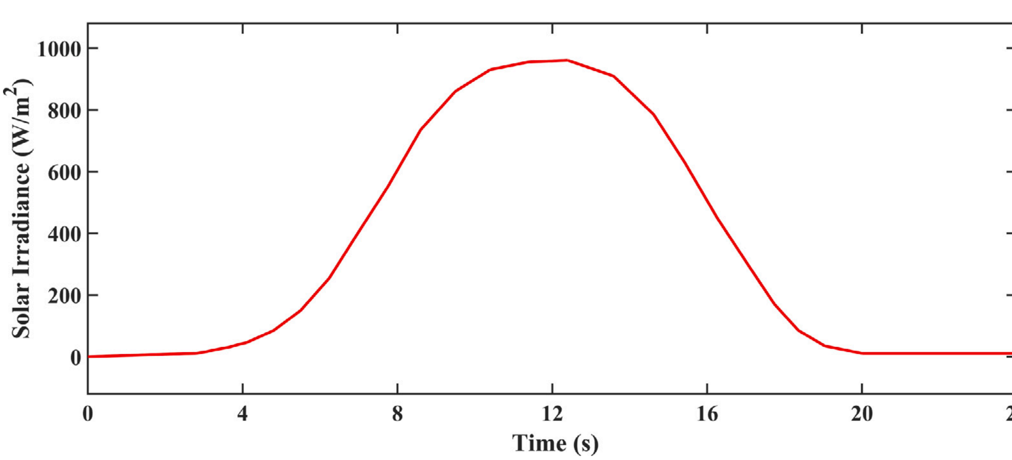

Fig. 9. Irradiance profile changes with time.

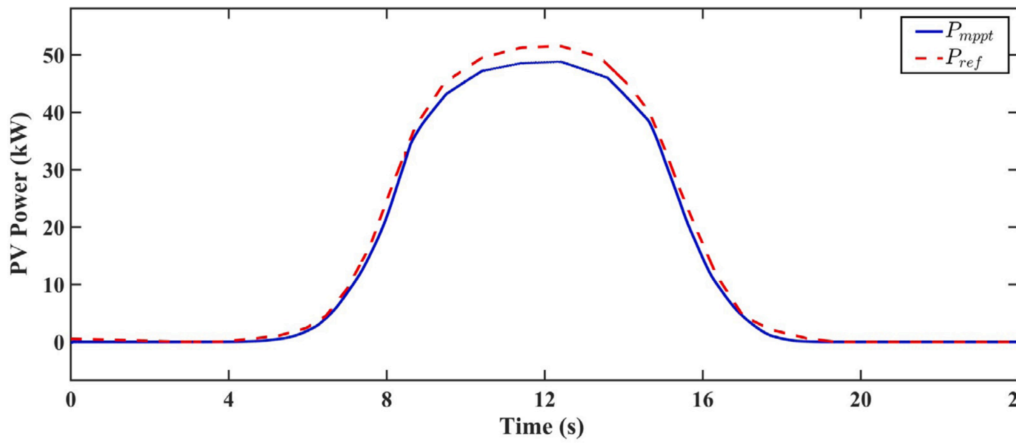

Fig. 10. PV power.

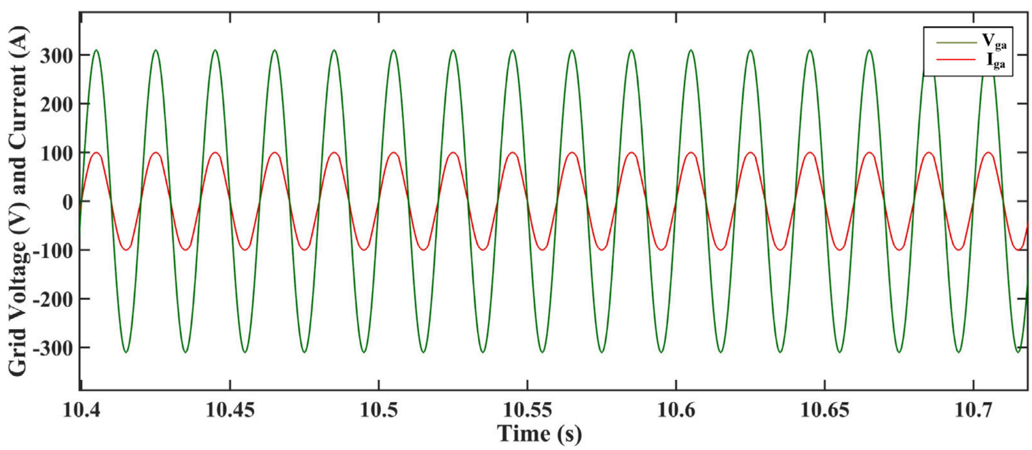

Fig. 11. Grid phase 'a' voltage and current.

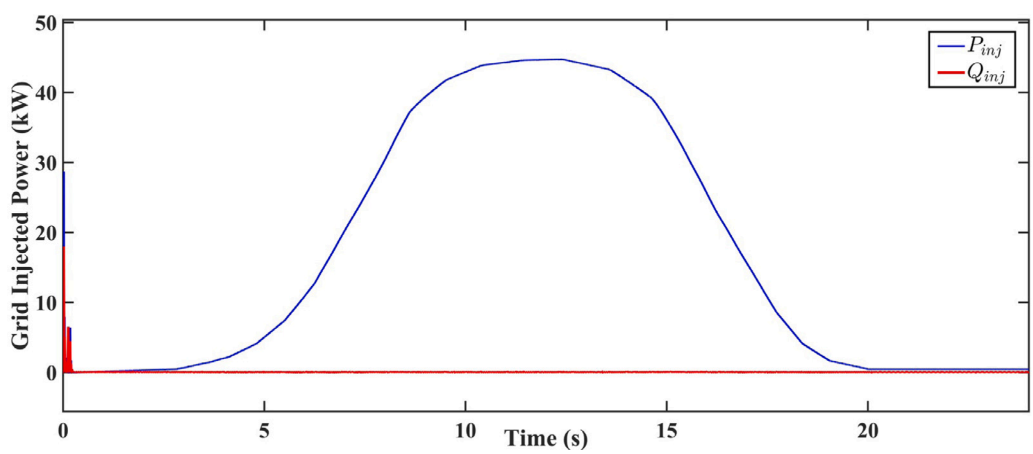

Fig. 12. Active and reactive power injected into the grid.

The result of the observer is compared with the actual states of the system under the proposed control technique. The estimated value will be utilized by the proposed controller.

The observer with the proposed technique, AO-FTSMC accurately estimates the state x_1 grid current d-component (i_{gd}), state x_2 the voltage across capacitor d-component (v_{cd}) and state x_3 inverter output current d-component, which is shown in Fig. 24, Fig. 25, and Fig. 26 respectively. These estimates show that d-component of actual states and estimated states matched well.

Figs. 27–29 show the actual states (grid Current i_{gq}, voltage across the capacitor v_{cq}, inverter Output Current i_{iq}) and estimated states ($\hat{i}_{gq}$, $\hat{v}_{cq}$, $\hat{i}_{iq}$), which are matched as well. As i_q reference equals zero, the estimated state $\hat{i}_{gq}$, accurately tracks the actual state i_{gq}.

4.5. Comparative analysis

The proposed control techniques are compared with the conventional P&O based PI MPPT algorithms. The ratio of the PV output power

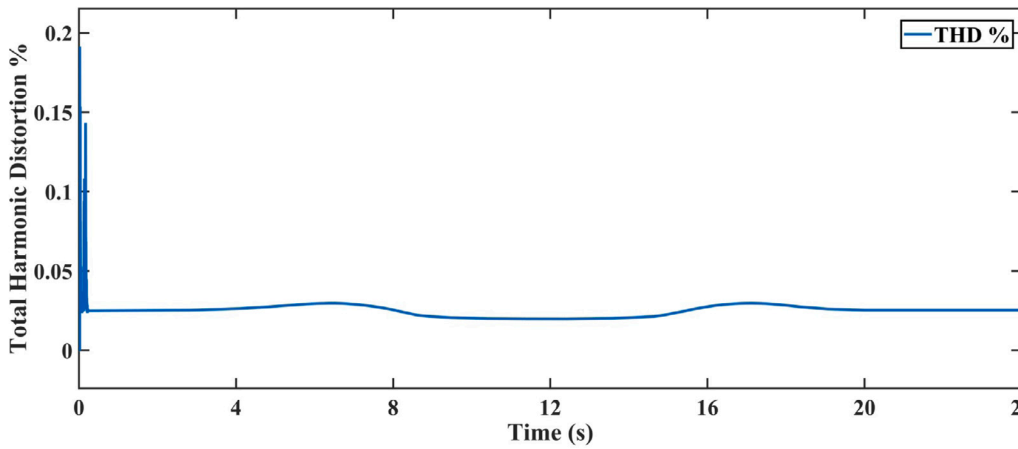

Fig. 13. Total harmonic distortion.

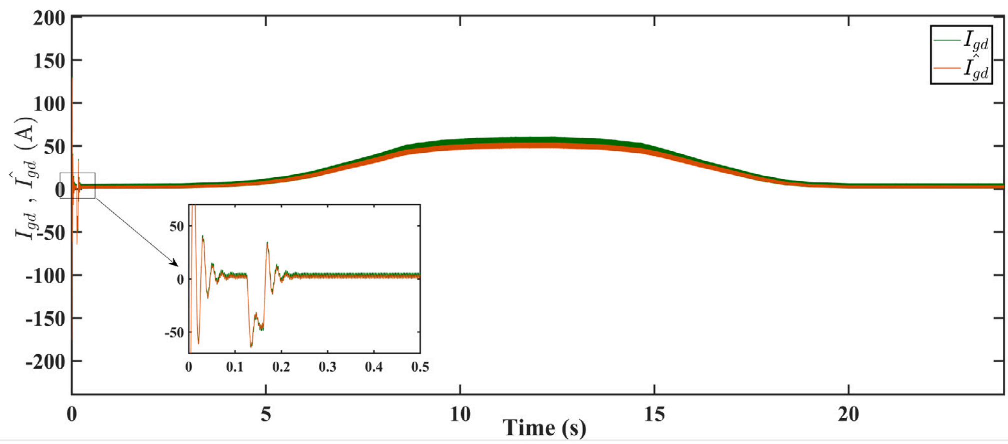

Fig. 14. Grid current d-component.

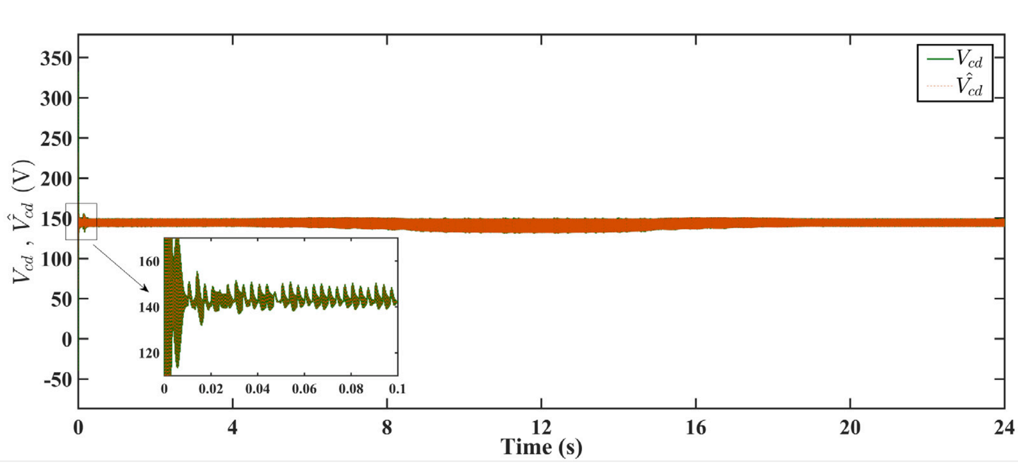

Fig. 15. Voltage across filter capacitor d-component.

to the reference power over a specific time period is known as dynamic efficiency.

$$\eta_{100} = \frac{\int_{t_0}^{t_f} P_{\mathrm{PV}}\,dt}{\int_{t_0}^{t_f} P_{\mathrm{PV\text{-}ref}}\,dt} \times 100 = \frac{\int_{t_0}^{t_f} (V_{\mathrm{PV}} \times I_{\mathrm{PV}})\,dt}{\int_{t_0}^{t_f} P_{\mathrm{PV\text{-}ref}}\,dt} \times 100 \tag{44}$$

The η_{100} is the present dynamic efficiency and $t_0 = 0$ and $t_f = 24s$ are the initial and final time, respectively. Fig. 30 displays the PV's dynamic efficiency. That is described in the following scenario.

Fig. 30 shows the efficiency of the proposed control techniques and the conventional MPPT strategy. The STR-FTSMC has an efficiency of 92.31% and AO-FTSMC has an efficiency of 98.19% while P&O-PI has an efficiency of 91.85%. The PV output power of all three algorithms are compared in Fig. 31. It is obvious from the figure that AO-FTSMC outperforms and it tracks the reference maximum power closely, accurately and smoothly with rapid variation in the PV output power. The real power injected into the grid is depicted in Fig. 32.

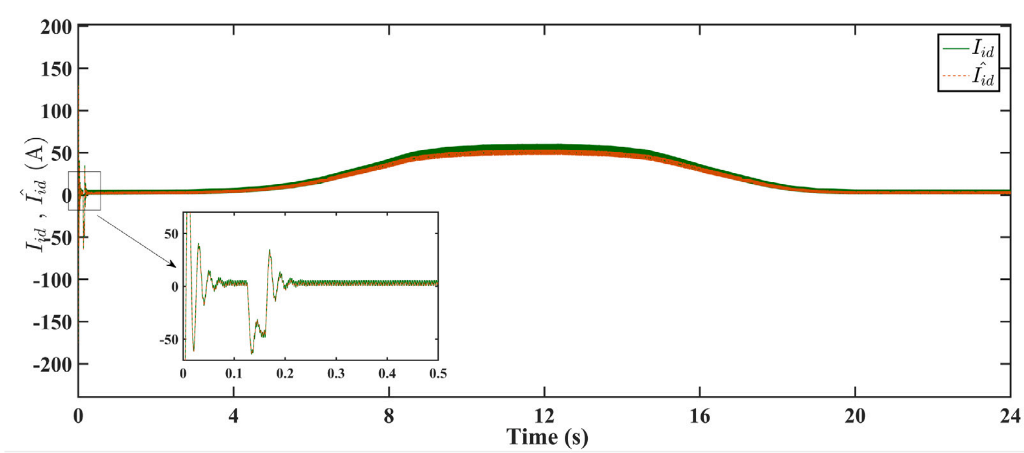

Fig. 16. Inverter output current d-component.

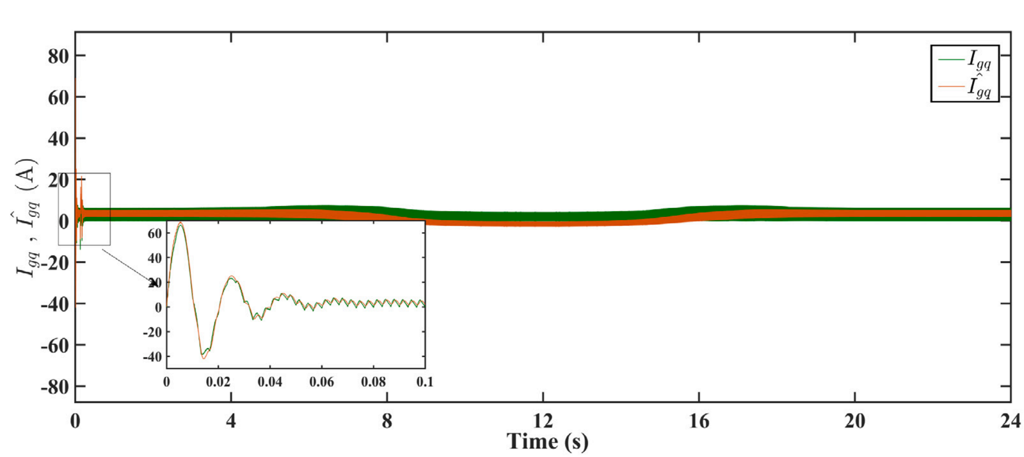

Fig. 17. Grid current q-component.

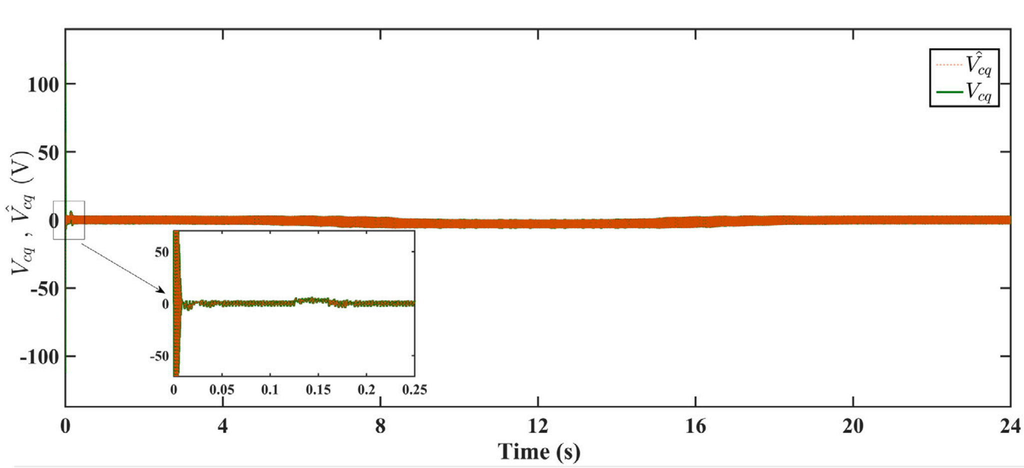

Fig. 18. Voltage across filter capacitor q-component.

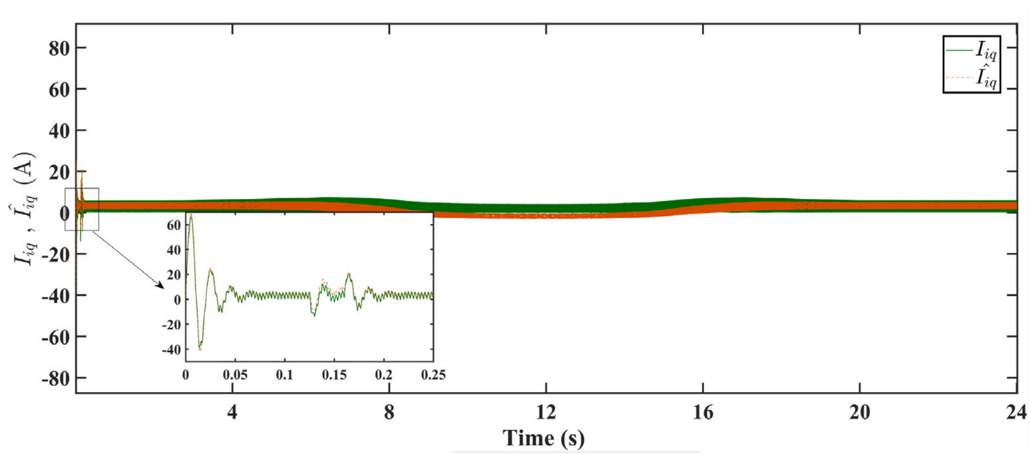

Fig. 19. Inverter output current q-component.

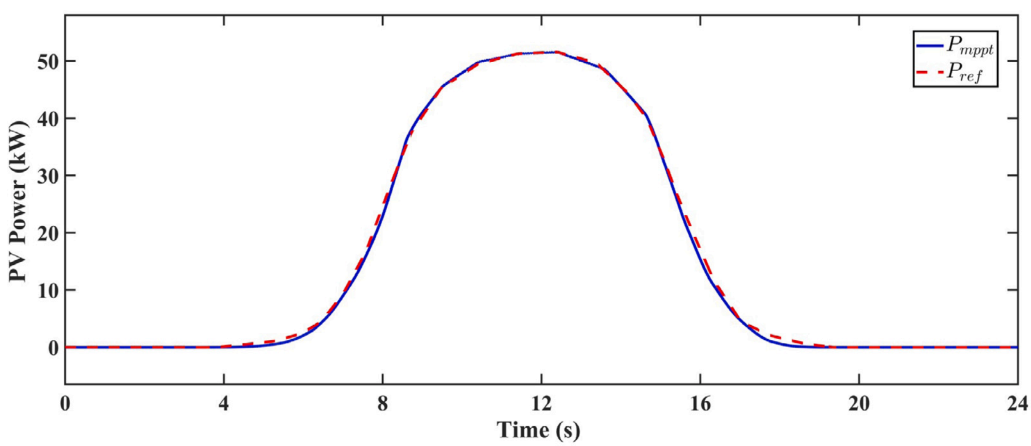

Fig. 20. PV power.

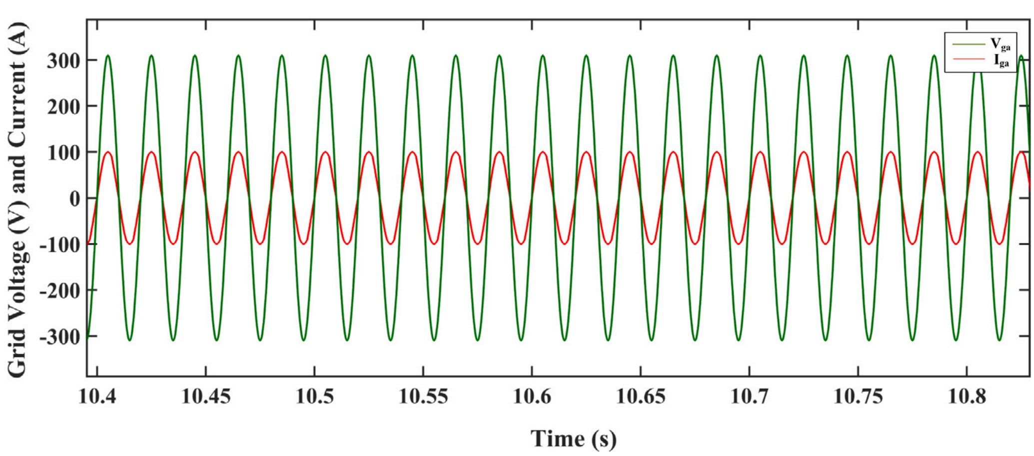

Fig. 21. Grid phase ‘a’ voltage and current.

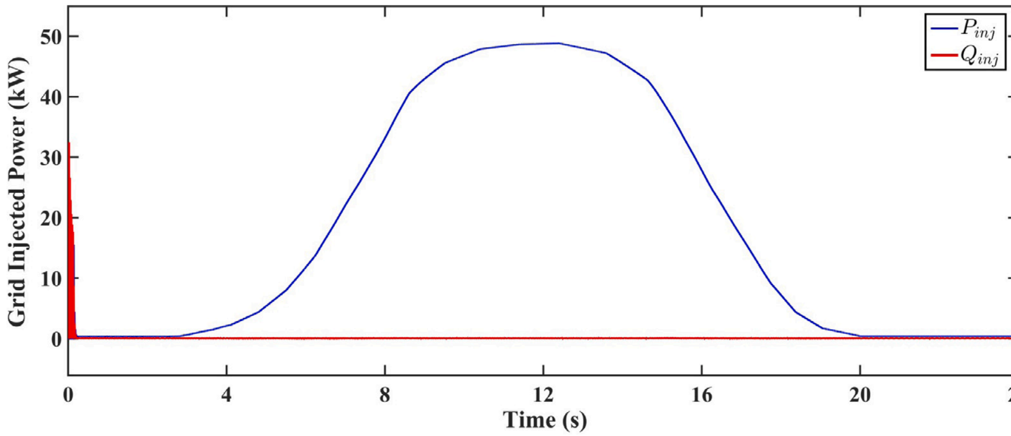

Fig. 22. Active and reactive power injected into the grid.

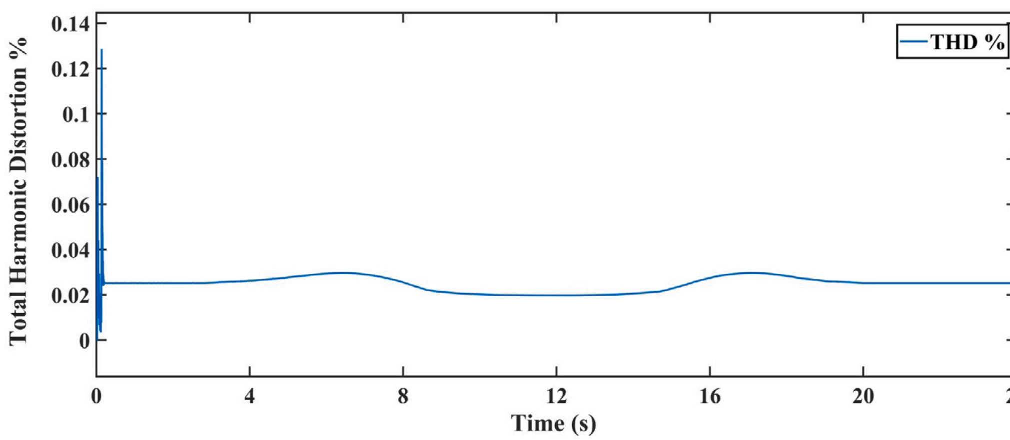

Fig. 23. Total harmonic distortion.

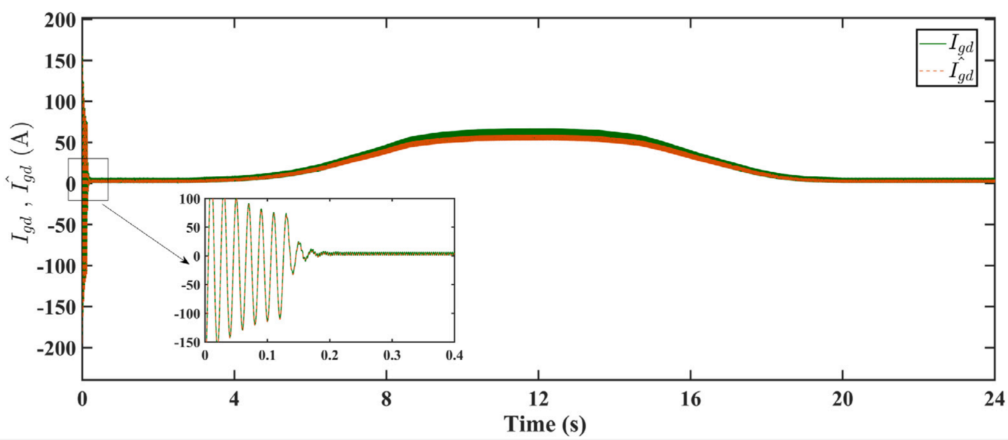

Fig. 24. Grid current d-component.

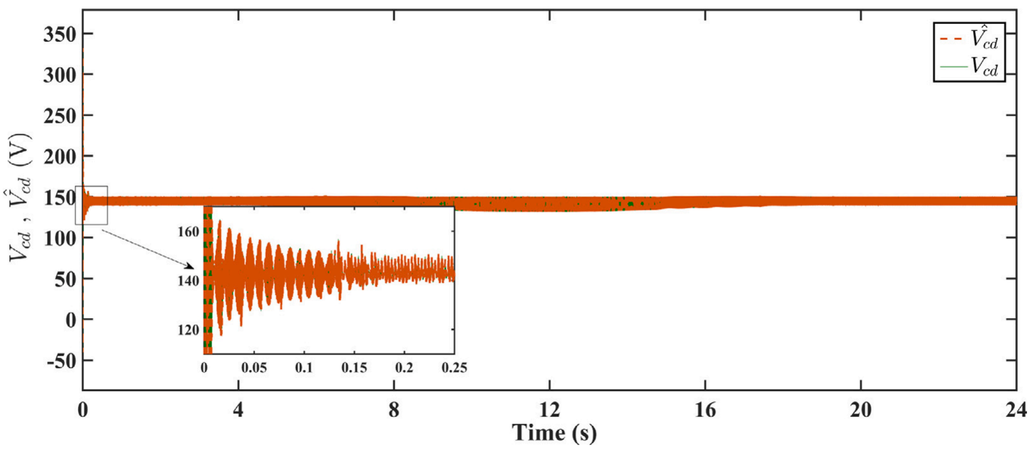

Fig. 25. Voltage across filter capacitor d-component.

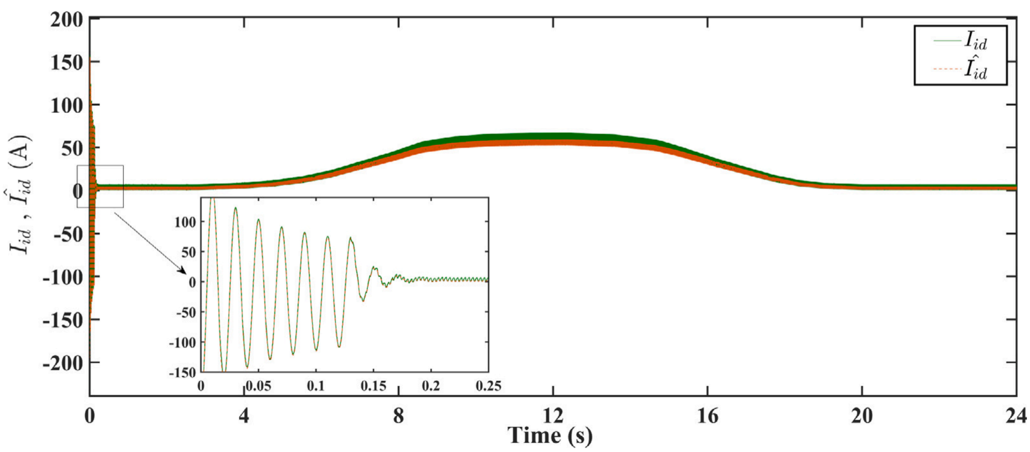

Fig. 26. Inverter output current d-component.

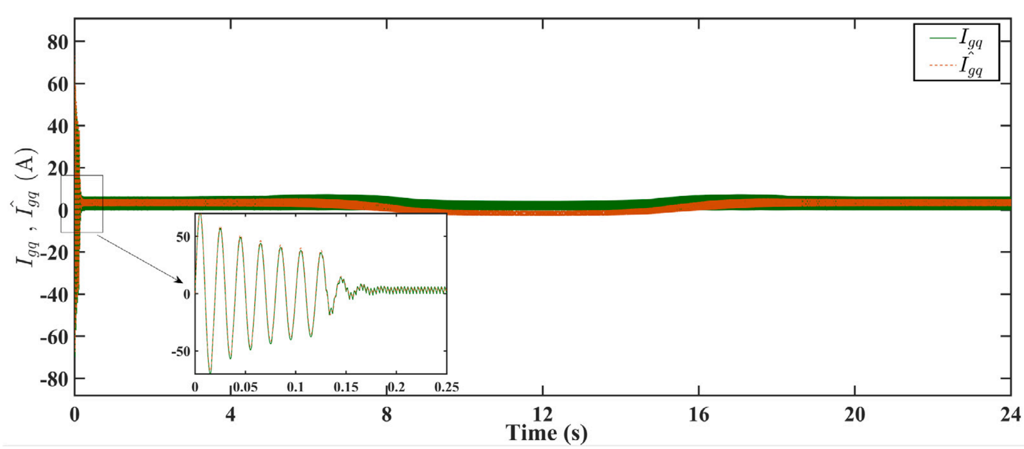

Fig. 27. Grid current q-component.

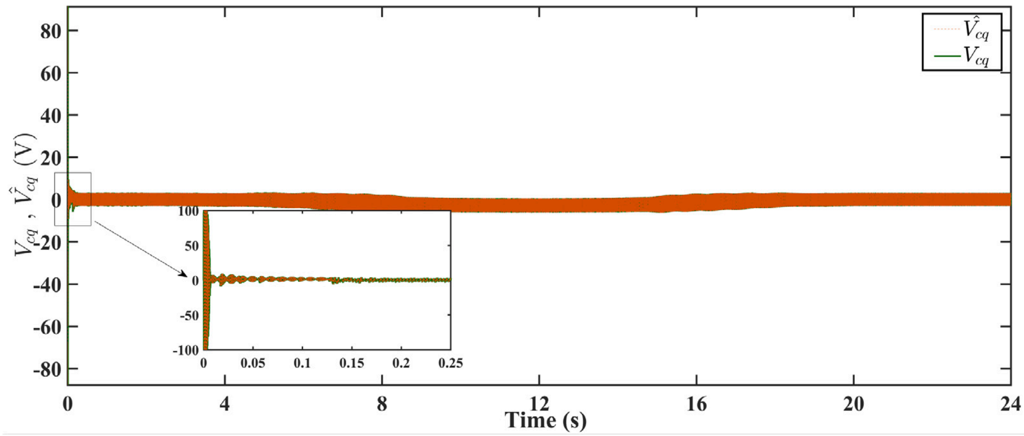

Fig. 28. Voltage across filter capacitor q-component.

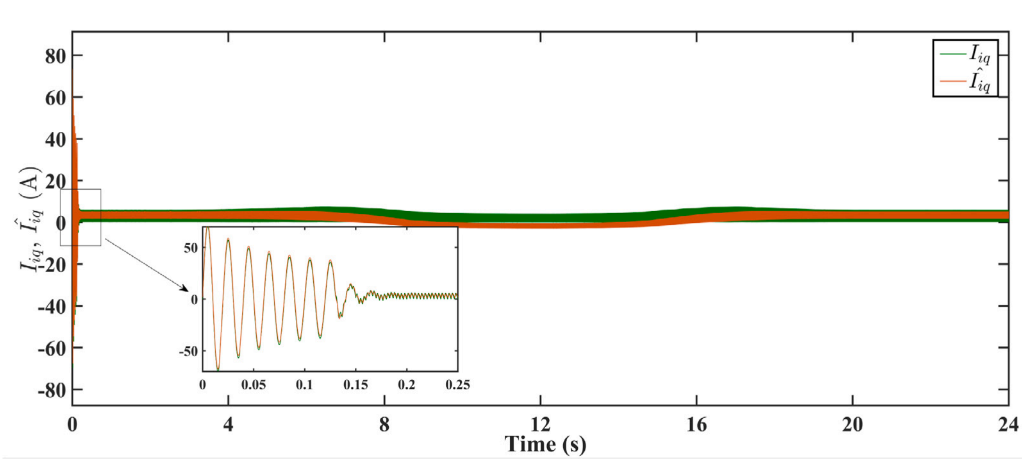

Fig. 29. Inverter output current q-component.

The AO-FTSMC outperforms both the STR-FTSMC and the conventional P&O-PI. It is observed that the AO-FTSMC injects clean active power into the grid and maximum power is dumped into the grid as compared to STR-FTSMC and P&O-PI. The active power into the grid by the P&O-PI is accompanied by chattering. Fig. 33 gives a percent THD comparison of the proposed and conventional technique. It is obvious from the figure that THD of the proposed control techniques is better than the conventional one. Although the %THD of the conventional P&O-PI is high but in the time interval 7–17 s, it is within the IEEE standard limit $\leq 5\%$.

Based on the analysis given above, AO-FTSMC has outperformed both STR-FTSMC and P&O-PI in terms of maximum power extraction, grid power injection, dynamic efficiency and THD.

5. Conclusion

In this paper, a single-stage 3-phase grid connected PV system is used to inject maximum real power extracted from PV arrays with low THD. The observer based proposed nonlinear techniques, AO-FTSMC outperforms ST-FTSMC and P&O-PI, in term of achieving maximum power extraction, high efficiency and very low THD. The Uktin observer adequately estimates the unavailable states from the grid currents. The performance of the proposed Uktin observer based MPPT paradigms is validated using MATLAB/Simulink. AO-FTSMC injects maximum real power into the grid at 98.19% efficiency and 0.0252% THD as compared to ST-FTSMC with ($\eta_{100} = 92.31\%,\ \%THD = 0.0252$) and P&O with ($\eta_{100} = 91.58\%,\ \%THD = 4.9$).

CRediT authorship contribution statement

Ahmad Khan: Writing – original draft, Visualization, Validation, Software, Methodology, Conceptualization. **Laiq Khan:** Writing – review & editing, Visualization, Supervision, Project administration, Methodology, Investigation, Formal analysis, Conceptualization. **Qudrat Khan:** Writing – original draft, Validation, Supervision, Investigation, Formal analysis, Conceptualization. **Zahid Ullah:** Writing – review & editing, Writing – original draft, Resources, Project administration, Formal analysis. **Adil Latif:** Writing – original draft, Resources, Methodology, Investigation, Formal analysis, Data curation.

Declaration of competing interest

The authors declare that they have no known competing financial interests or personal relationships that could have appeared to influence the work reported in this paper.

Data availability

Data will be made available on request.

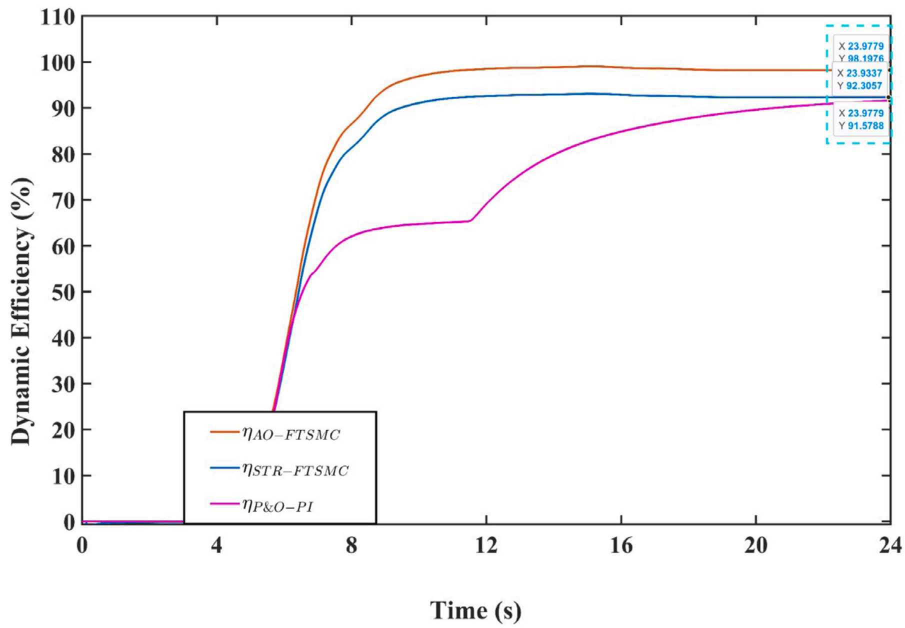

Fig. 30. Dynamic efficiency.

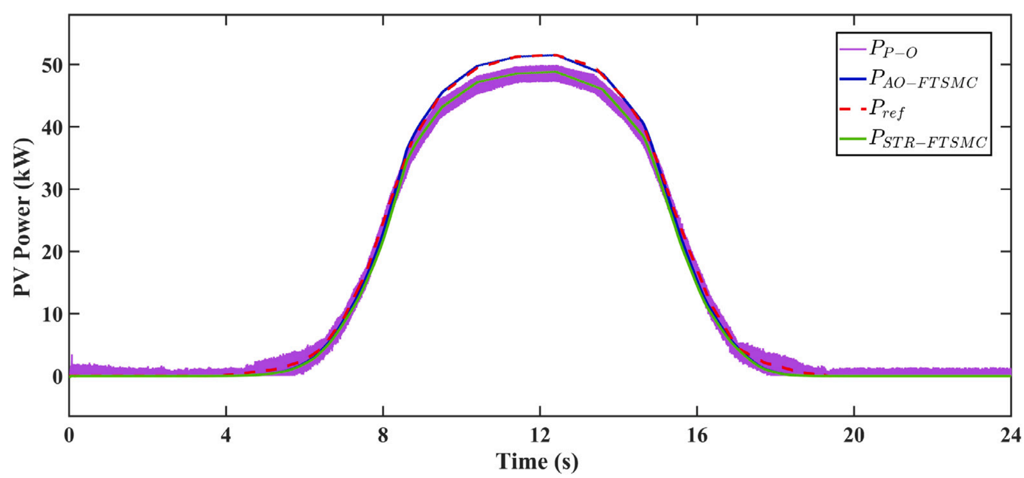

Fig. 31. PV power.

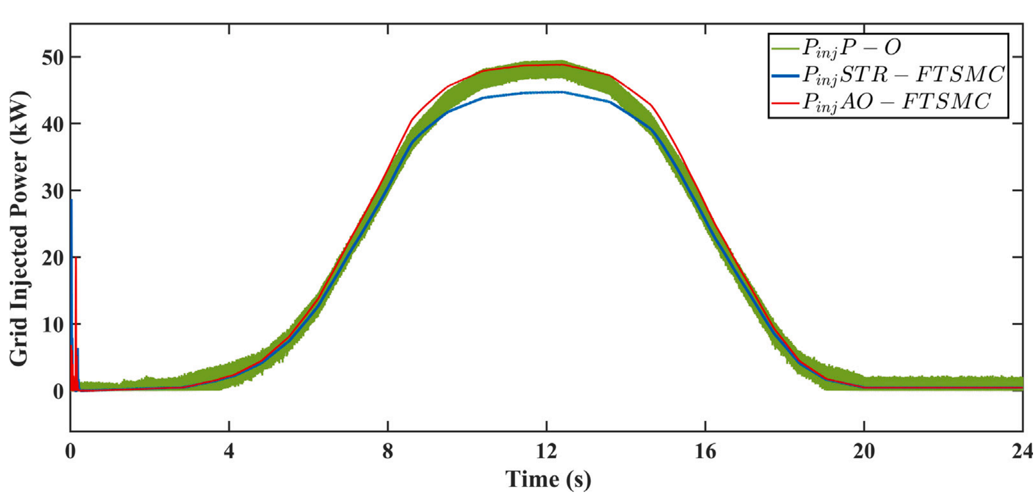

Fig. 32. Real power injected into the grid of AO-FTSMC and STR-FTSMC.

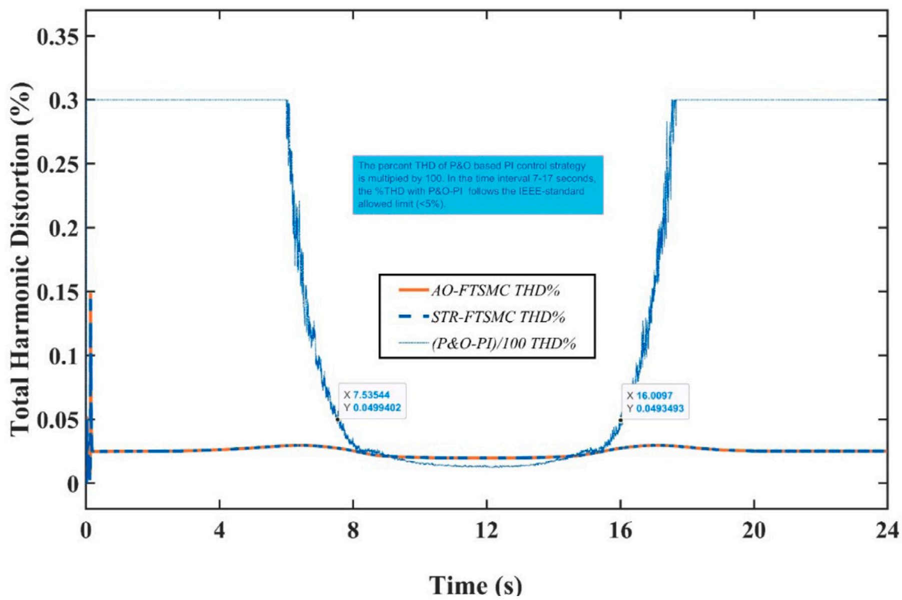

Fig. 33. Total harmonic distortion.

Appendix A. Supplementary equations

$$\left.\begin{aligned} v_{g_{abc}} &= T^{-1} v_{g_{dq}} \\ i_{i_{abc}} &= T^{-1} I_{i_{dq}} \\ v_{i_{abc}} &= T^{-1} v_{i_{dq}} \\ v_{c_{abc}} &= T^{-1} v_{c_{dq}} \end{aligned}\right\} \tag{1A}$$

where T is transformation matrix,

$$T = \frac{2}{3}\begin{bmatrix} cos\theta & cos(\theta - \frac{2\pi}{\theta}) & cos(\theta + \frac{2\pi}{\theta}) \\ -sin\theta & -sin(\theta - \frac{2\pi}{\theta}) & -sin(\theta + \frac{2\pi}{\theta}) \\ \frac{1}{2} & \frac{1}{2} & \frac{1}{2} \end{bmatrix} \tag{2A}$$

and,

$$T\frac{d}{dt}T^{-1} = \begin{bmatrix} 0 & -\omega & 0 \\ \omega & 0 & 0 \\ 0 & 0 & 0 \end{bmatrix} \tag{3A}$$

$$\left.\begin{aligned} \frac{d}{dt}T^{-1}v_{c_{dq}} &= \frac{1}{C}T^{-1}i_{i_{dq}} - \frac{1}{C}T^{-1}i_{g_{dq}} \\ \frac{d}{dt}T^{-1}i_{i_{dq}} &= \frac{1}{L_i}T^{-1}v_{i_{dq}} - \frac{1}{L_i}T^{-1}v_{c_{dq}} \\ \frac{d}{dt}T^{-1}i_{g_{dq}} &= \frac{1}{L_g}T^{-1}v_{c_{dq}} - \frac{1}{L_g}T^{-1}v_{g_{dq}} \end{aligned}\right\} \tag{4A}$$

Appendix B. System and observer matrices

$$A = \begin{bmatrix} 0 & \frac{1}{L_g} & 0 & \omega & 0 & 0 \\ -\frac{1}{C} & 0 & \frac{1}{C} & 0 & \omega & 0 \\ 0 & -\frac{1}{L_i} & 0 & 0 & 0 & \omega \\ -\omega & 0 & 0 & 0 & \frac{1}{L_g} & 0 \\ 0 & -\omega & 0 & -\frac{1}{C} & 0 & \frac{1}{C} \\ 0 & 0 & -\omega & 0 & -\frac{1}{L_i} & 0 \end{bmatrix}, B = \begin{bmatrix} 0 & 0 \\ 0 & 0 \\ \frac{1}{L_i} & 0 \\ 0 & 0 \\ 0 & 0 \\ 0 & \frac{1}{L_i} \end{bmatrix}, C = \begin{bmatrix} 1 & 0 \\ 0 & 0 \\ 0 & 0 \\ 0 & 1 \\ 0 & 0 \\ 0 & 0 \end{bmatrix}^T$$

$$L = \begin{bmatrix} L_{11} & . & . & L_{1n} \\ . & . & . & . \\ . & . & . & . \\ L_{m1} & . & . & L_{mn} \end{bmatrix}, G = \begin{bmatrix} G_{11} & . & . & G_{1n} \\ . & . & . & . \\ . & . & . & . \\ G_{m1} & . & . & G_{mn} \end{bmatrix}$$

References

Alam, W., Khan, Q., Riaz, R.A., Akmeliawati, R., 2020. Arbitrary-order sliding mode-based robust control algorithm for the developing artificial pancreas mechanism. IET Syst. Biol. 14 (6), 307–313.

Bao, C., Ruan, X., Wang, X., Li, W., Pan, D., Weng, K., 2013. Step-by-step controller design for LCL-type grid-connected inverter with capacitor–current-feedback active-damping. IEEE Trans. Power Electron. 29 (3), 1239–1253.

Barzegar-Kalashani, M., Mahmud, M.A., Tousi, B., Farhadi-Kangarlu, M., 2023. A step-by-step full-order sliding mode controller design for standalone inverter-interfaced cleaner renewable energy sources. Clean. Energy Syst. 6, 100080.

Barzegar-Kalashani, M., Tousi, B., Mahmud, M.A., Farhadi-Kangarlu, M., 2022. Robust nonlinear sliding mode controllers for single-phase inverter interfaced distributed energy resources based on super twisting algorithms. ISA Trans. 123, 61–75.

Benyoucef, A., Kara, K., Chouder, A., Silvestre, S., 2014. Prediction-based deadbeat control for grid-connected inverter with L-filter and LCL-filter. Electr. Power Compon. Syst. 42 (12), 1266–1277.

Beres, R.N., Wang, X., Liserre, M., Blaabjerg, F., Bak, C.L., 2015. A review of passive power filters for three-phase grid-connected voltage-source converters. IEEE J. Emerg. Sel. Top. Power Electron. 4 (1), 54–69.

Blaabjerg, F., Teodorescu, R., Liserre, M., Timbus, A.V., 2006. Overview of control and grid synchronization for distributed power generation systems. IEEE Trans. Ind. Electron. 53 (5), 1398–1409.

Bo, Q., Xiao-yuan, H., Wen-xi, Y., Zheng-yu, L., Guerrero, J.M., 2009. An optimized deadbeat control scheme using fuzzy control in three-phase voltage source PWM rectifier. In: 2009 Twenty-Fourth Annual IEEE Applied Power Electronics Conference and Exposition. IEEE, pp. 1215–1219.

Chigane, K., Ouassaid, M., 2024. Experimental assessment of integral-type terminal sliding mode control designed for a single-phase grid-interlinked PV system. Control Eng. Pract. 147, 105903.

Dehkordi, N.M., Sadati, N., Hamzeh, M., 2016. A robust backstepping high-order sliding mode control strategy for grid-connected DG units with harmonic/interharmonic current compensation capability. IEEE Trans. Sustain. Energy 8 (2), 561–572.

Drakunov, S.V., Utkin, V.I., 1992. Sliding mode control in dynamic systems. Int. J. Control 55 (4), 1029–1037.

Esram, T., Chapman, P.L., 2007. Comparison of photovoltaic array maximum power point tracking techniques. IEEE Trans. Energy Convers. 22 (2), 439–449.

Hao, X., Yang, X., Liu, T., Huang, L., Chen, W., 2012. A sliding-mode controller with multiresonant sliding surface for single-phase grid-connected VSI with an LCL filter. IEEE Trans. Power Electron. 28 (5), 2259–2268.

Huang, M., Li, H., Wu, W., Blaabjerg, F., 2019. Observer-based sliding mode control to improve stability of three-phase LCL-filtered grid-connected VSIs. Energies 12 (8), 1421.

Husev, O., Roncero-Clemente, C., Makovenko, E., Pimentel, S.P., Vinnikov, D., Martins, J., 2019. Optimization and implementation of the proportional-resonant controller for grid-connected inverter with significant computation delay. IEEE Trans. Ind. Electron. 67 (2), 1201–1211.

Jamil, M., Waris, A., Gilani, S.O., Khawaja, B.A., Khan, M.N., Raza, A., 2020. Design of robust higher-order repetitive controller using phase lead compensator. IEEE Access 8, 30603–30614.
Kale, M., Karabacak, M., Kruschel, W., Kilic, F., Zacharias, P., 2016. Chattering free robust control of LCL filter based shunt active power filter using adaptive second order sliding mode and resonant controllers. Int. J. Electr. Power Energy Syst. 76, 174–184.
Kim, I.S., 2006. Sliding mode controller for the single-phase grid-connected photovoltaic system. Appl. Energy 83 (10), 1101–1115.
Kim, I.S., 2007. Robust maximum power point tracker using sliding mode controller for the three-phase grid-connected photovoltaic system. Sol. Energy 81 (3), 405–414.
Komurcugil, H., Ozdemir, S., Sefa, I., Altin, N., Kukrer, O., 2015. Sliding-mode control for single-phase grid-connected LCL-filtered VSI with double-band hysteresis scheme. IEEE Trans. Ind. Electron. 63 (2), 864–873.
Levant, A., 1993. Sliding order and sliding accuracy in sliding mode control. Int. J. Control 58 (6), 1247–1263.
Mahmud, M.A., Pota, H.R., Hossain, M.J., Roy, N.K., 2013. Robust partial feedback linearizing stabilization scheme for three-phase grid-connected photovoltaic systems. IEEE J. Photovolt. 4 (1), 423–431.
Menaga, D., Sankaranarayanan, V., 2020. A novel nonlinear sliding mode controller for a single stage grid-connected photovoltaic system. ISA Trans. 107, 329–339.
Naddami, S., Ababssi, N., 2023. Power quality optimization using a novel backstepping control of a three-phase grid-connected photovoltaic systems. Int. J. Electr. Comput. Eng. (IJECE) 13 (3), 2517–2528.
Rivera, P.R., McIntyre, M.L., Mohebbi, M., Latham, J., 2017. Single—Stage three—Phase grid—Connected photovoltaic system with maximum power tracking and active and reactive power control based on nonlinear control. In: 2017 IEEE Energy Conversion Congress and Exposition. ECCE, IEEE, pp. 1–7.
Ullah, A., Khan, L., Khan, Q., 2020. Variable gain real-twisting sliding mode M PPT control for permanent magnet synchronous generator based wind energy conversion system. In: 2020 3rd International Conference on Computing, Mathematics and Engineering Technologies. iCoMET, IEEE, pp. 1–7.
Vieira, R.P., Martins, L.T., Massing, J.R., Stefanello, M., 2017. Sliding mode controller in a multiloop framework for a grid-connected VSI with LCL filter. IEEE Trans. Ind. Electron. 65 (6), 4714–4723.
Wu, T.F., Chang, C.H., Lin, L.C., Kuo, C.L., 2011. Power loss comparison of single-and two-stage grid-connected photovoltaic systems. IEEE Trans. Energy Convers. 26 (2), 707–715.
Wu, W., He, Y., Tang, T., Blaabjerg, F., 2012. A new design method for the passive damped LCL and LLCL filter-based single-phase grid-tied inverter. IEEE Trans. Ind. Electron. 60 (10), 4339–4350.
Yu, X., Feng, Y., Man, Z., 2020. Terminal sliding mode control – An overview. IEEE Open J. Ind. Electron. Soc. 36–52. http://dx.doi.org/10.1109/ojies.2020.3040412.
Yuan, L., Xiu, C., Ma, X., 2023. Sliding mode control strategy for microgrid inverter systems. J. Power Electron. 23 (5), 821–831.
Zeb, K., Busarello, T.D., Ul Islam, S., Uddin, W., Raghavendra, K.V., Khan, M.A., Kim, H.J., et al., 2020. Design of super twisting sliding mode controller for a three-phase grid-connected photovoltaic system under normal and abnormal conditions. Energies 13 (15), 3773.
Zeb, K., Uddin, W., Khan, I., Ishfaq, M., Ullah, Z., Busarello, T.D., Kim, H.J., 2019. Design of adaptive sliding mode controller for single-phase grid-tied PV system. In: 2019 15th International Conference on Emerging Technologies. ICET, IEEE, pp. 1–6.
Zeb, K., Uddin, W., Khan, I., Khan, M.A., Ullah, Z., Kim, H.J., 2018. A novel design of FRT strategy and proportional resonant controller for three phase grid connected PV system. In: 2018 International Conference on Power Generation Systems and Renewable Energy Technologies. PGSRET, IEEE, pp. 1–6.
Zhang, Q., Song, X., Song, S., Stojanovic, V., 2023. Finite-time sliding mode control for singularly perturbed PDE systems. J. Franklin Inst. 360 (2), 841–861.